NASA CONTRACTOR
REPORT

NASA CR-884
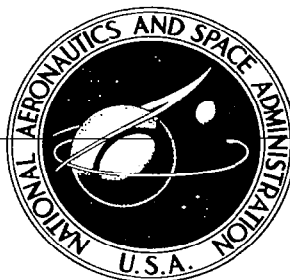
N.A.S.A. CR-

VIBRATION STUDY OF A PRESSURIZED TORUS SHELL

Part I - Experimental Study ·

by Peter F. Jordan

Prepared by
MARTIN COMPANY
Baltimore, Md.
for Langley Research Center

NASA CR-661

VIBRATION STUDY OF A PRESSURIZED TORUS SHELL

Part I - Experimental Study

By Peter F. Jordan

NATIONAL AERONAUTICS AND SPACE ADMINISTRATION

FOREWORD

This report comprises the experimental portion of a two-part vibration study of a pressurized torus shell and was presented in part at the AIAA 5th Aerospace Sciences Meeting in New York, New York, January 23-26, 1967 (AIAA Paper No. 67-73). Part II of this study, which is given in NASA CR-885, contains the development and applications of a torus shell vibration analysis prepared by Atis A. Liepins of the Dynatech Corp., Cambridge, Massachusetts, under Contract No. NAS 1-6632.

CONTENTS

VIBRATION STUDY OF A PRESSURIZED TORUS SHELL
Part I — Experimental Study

By Peter F. Jordan
Martin Company

SUMMARY

Results of a vibration test program performed on a 54-inch (1.4 m) diameter complete circular torus shell are reported. The fundamental frequency response of both the free and the rigidly held model agreed well with analytical predictions. Correlation of the higher frequency modal responses by means of results of cylindrical shell analysis was successful in general, though pneumatic resonances of the air inside the model also played a considerable role. Significant was the occurrence of nonclassical modes, of a high degree of symmetry and evidently not due to model imperfections.

INTRODUCTION

The problem of the static analysis of thin-walled, pressurized toroidal shell configurations can be considered resolved in principle. A static test program, reported in ref. 1, confirmed the validity of an asymptotic form of this analysis. This asymptotic analysis, though it is unexpectedly compact, is nevertheless sufficiently accurate for engineering purposes in the parameter range of most space type applications, and proved useful also in the present shell vibration program.

Regarding the dynamic problem of the response of a torus shell to vibratory excitation, a sizeable set of numerical analysis results has been presented by Liepins in refs. 2 and 3, and some interpolative relations, derived from asymptotic static analysis, have been given by Jordan in ref. 4. The purpose of the investigation presented here was to obtain experimental evidence and to relate the experimental results to analytical predictions as far as this was readily feasible without, however, taking recourse to performing actual shell vibration analyses.

The structural model that we used in this experimental investigation was the complete circular torus shell which we had manufactured for the static testing program (ref. 1) and had used therein. By looking briefly at Figures 1 through 6, the reader will obtain a survey of model parameters, model design, and test arrangement for the present program.

The model was tested under two basic supporting conditions, "fixed" and "free". In the former, it was held rigidly, supposedly, along its outer circumference; in the latter, it was carried by a soft suspension to its hub. Primary pressurization levels selected were p = 0* (the unpressurized shell), p = 6 (shell bending stiffness and stiffness due to

*For brevity, a given internal pressurization level p is described simply by a number in the text of this report. This number gives the difference between internal air pressure and external air pressure in lb/in.^{2}. Translation into kg/cm^2 is given in Table II. Similarly, all frequencies are denoted by numbers only; for example, f = 140 means a frequency of 140 cps = 140 Hz.

pressure about equal) and p = 15 (the model behavior under a static load approaches that of a pressurized membrane shell).

In a number of respects, our undertaking corresponded to the investigation of a pressurized cylindrical shell that is reported in ref. 5; indeed, a cylindrical shell is a torus shell having the opening ratio a = ∞. A fairly straightforward test procedure had been visualized for our program: resonances would be excited, the nodal pattern of each would be made visible by means of semi-sticking powder and the vibration mode would thus be identified, simply by counting, in a manner corresponding to that used in the case of cylindrical shells, the number of meridional nodes (nodes that form a meridional circle) and of circumferential nodes (nodes that form a circle around the torus axis). Finally, the meridional modal shape would be determined in detail for a few of the lowest modes.

Certain complications were expected, of course. There would be split modes*, and it would be necessary to experiment with the excitation arrangement to determine effects of exciter location and type. The complications that actually arose went far beyond those expected. There were none with regard to the fundamental mode, which had both the frequency and the modal shape that was predicted by the asymptotic static analysis. However, the spectrum beyond the second analytically predicted overtone, which was the first observed overtone, was quite crowded; in some modes the nodal lines had a pronounced tendency to deviate from the expected "classical" nodal pattern of two sets of complete circles; there was often a continuous shift of the phase angle of the shell vibration along the shell and no proper nodal line; furthermore, there were often relatively large amplitudes of harmonic (usually in the next higher octave) motions. In consequence, it sometimes became difficult or impossible to identify the individual modes.

This was first observed with the "fixed" model. Noting that variations of neither exciter location nor direction helped and noting further that the model supporting fixture, Figure 4, was not, in effect, as rigid as it had been supposed to be (it took part in the vibration to a considerable degree) we next changed over to the "free" model. This did not eliminate all sources of concern, but it helped to clarify them. It eliminated a rather undefined source of resonances but, of course, added torus modes proper that had been suppressed on the "fixed" model. It eliminated most of the previous response in higher harmonics. It did not eliminate the nonclassical modes but rather proved them to be an inherent property of the torus shell configuration. It did not eliminate the annoying phase shifts, and may even have increased them; however, the occurrence of large resonance responses where the torus shell oscillated, as an (almost) rigid body, against the stiffness produced by a pneumatic resonance of the air inside the torus shell, gave a hint that some of the observed phase shifts may have been produced by pneumatic coupling.

There were thus two unexpected phenomena: nonclassical modes and pneumatic modes. There were, apart from these, sufficiently clean overtone modes that had to be related to the analysis of a shell vibrating in a vacuum. It became apparent, however, that an insufficient number of specific analytical results (ref. 3) was available for this purpose, and a different approach was tried, namely, correlation to cylindrical shell vibration analysis. The ordering principle that was devised for this purpose turned out to be satisfactory.

*Due to an imperfection of the model, a resonance mode of the ideal model may be split into two modes having slightly different frequencies. Compare, e.g., ref. 6.

In this paper, the test program is first described. Next, analysis procedure and results are given for the fundamental mode. A discussion of the nature of torus shell overtone modes follows, a listing of Liepins' applicable results (ref. 3), and a derivation of the correlation to cylindrical shells. The next section is concerned with the pneumatic modes. On this basis, finally, our test results for shell overtone modes are discussed: first the first overtone mode, which has some interesting features of its own, then the frequency spectra, the photographic records, the modal deflections measured, and the detailed correlations to cylindrical shell vibration analysis and to predictions of internal pneumatic resonances.

It should be stressed that the present investigation, insofar as it led to unexpected observations, brought up a number of most interesting questions which could not, however, have been resolved to satisfaction during this program. Neither was the test set-up planned for this purpose, nor was the test time available. In these respects, our effort has to be considered as exploratory, and some of our conclusions as preliminary. Indeed, the present report represents a selection, necessary but sometimes difficult to make, from what seemed at times an overabundance of not always easily reconcilable bits of test information. Recommendations for further research are made in the concluding section.

TEST PROGRAM

The Model

The model that we used in our vibration test program was a complete circular torus shell. In Figure 1 some of the notation to be used is indicated, and also the static load system P under which the same model had been tested previously (ref. 1). (The then statically measured stiffness, S, was used to predict fundamental vibration frequencies; see below.) Model dimensions and manufacturing technique are indicated in Figure 2. The model was explosively formed from preforms welded from 2219-0 bare aluminum; Figure 2 shows the lower half before explosive forming. Figure 3 is a top view schematic, showing all the weld lines and also the positions of the ports, short lengths of tubing, for pressurization and for strain gage leads. Note, Figure 2, that the inner part of the model had been strengthened, as required by the pressurization stresses, and that the center (hub) of the torus shape proper had been closed. Upper and lower hub cups were held together by bolt and washers. Also, the weld connection along the outer circumference, Figure 1, incorporated an additional sheet metal ring inside the model.

Table I gives the average values of the model parameters that were used in the analyses. The thickness hR is that of the unstrengthened part of the model (to be exact, hR is the mean of the thicknesses that were measured along the two crowns*). Note that the opening ratio a (see Figure 1) is fairly small, making our model correspond more to a booster tank than to a space station.

Figure 2 also indicates the cylindrical structure that held the model in its "fixed" position. This support is shown in Figure 4. The cylinder had been formed from 3/8 inch (9.5 mm) steel plate; the ring at its top was 27/16 inch (43 mm) wide and 23/16 inch (37 mm) high. Connection to the model was provided via 100 T-shaped lugs, well visible in Figures 4 and 5; hard rubber plates had been cemented between lugs and model.

---

*After explosive forming. There was no recognizable effect of explosive forming on the thickness distribution.

The model had been instrumented with strain gages along the meridian $\theta = 0°$, Figures 2 to 4.

Model weights are given below in the section on fundamental modes. In some "fixed" tests, a heavy weight, about doubling the effective model mass, was attached to the model hub.

For the tests with the "free" model, the T-shaped lugs were taken off, but the model was left in about its previous position, as can be seen in most of the photographs, Figure 16. It was then carried by a soft rubber cord to its center, also visible in Figure 16. In this condition, all its suspension frequencies were around f = 1, while the lowest fundamental model frequency was f = 24.

Test Procedure

Figure 4 shows the overall test setup. The electrodynamic shaker, better visible in Figure 5, was attached to the shell through a light weight forcing bar, bonded to the shell surface with dental cement. The main shaker positions tried were: vertical at the hub for the fundamental modes; excitation directly at the crown ($\phi = 0°$ or $180°$, Figure 1) or $9°$ outside it, usually at $\theta = 180°$ around the circumference, Figure 3, in the "free" condition at the lower crown in order to minimize distortions on the top half of the shell, where observation was easiest, but at the upper crown in the "fixed" condition where excitation from the lower crown did not readily reach the top half shell, in particular at higher frequencies. Horizontal excitation at the outer circumference was tried; this attempt to bring out symmetrical modes was not very successful because of the smallness of the local modal amplitudes.

The shaker force applied was of the order ± 2.2 lb (1 kg) and was nearly always directed normal to the shell. During the test program, the bending stiffness of the forcing bar was considerably reduced by making two pairs of deep notches in order to eliminate possible distorting inputs. No effect of this weakening was found.

The model response (rms) was recorded as a function of frequency (spectrum plots) in terms of the output of either the distance detector, Figure 5, one of the strain gages, or the pressure transducer (which had been installed close to the model and connected to the internal pressurization tube). The upper limit of a frequency sweep was usually 1000 cps (Hz). Sweeping was done at the rate of 4.5 min per octave. Reducing the rate further had no noticeable effect.

The strain gages were also monitored in order not to overtax the model strength. This, however, was not a real problem. Rather, the sound level as such and the fact that sound distortions tended to occur, usually suddenly, when the amplitude was increased, set a practical limit for the applicable excitation force.

With all frequencies of interest in the audible range, the human ear was a very useful tool, both as an indicator of the overall magnitude of a given resonance amplitude, for which the output of an individual pick-up is a rather poor measure, and as an indicator of occurrence and source of distortions. This source was sometimes one of the port tubes, Figure 3, starting a vibration of its own.

The maximum amplitude of the shell at a representative overtone vibration was of the order ± 0.002 inch (0.05 mm).

After a frequency sweep had been made, individual resonances were investigated. A hand-held probe, with its output shown on an oscilloscope, allowed us to find nodal lines, phase shifts and harmonic distortions of the shell motion with respect to the excitation force (shaker current). In theory, it could also be used, by determining the phase relations between upper half shell and lower half shell, to interpret a given reso-nance as either symmetric* or antisymmetric. In practice, this was not always possi-ble; often, for reasons explained below in the discussion of overtone modes, the lower half shell did not have a simultaneous equivalent resonance, but had instead a much smaller response, or a different type of response pattern, or large phase shifts, etc.

The nodal pattern on the top half shell was made visible by means of a semi-sticky powder**. We used a mixture of 8% (by volume) magnesium stearate and 92% ecco-spheres. This powder showed up nodal lines, even on the vertical parts of the shell surface; a sample application is seen in Figure 4. Of course, effectiveness of this visual-ization requires a minimum of vibratory acceleration of the shell. The minimum fre-quency where this acceleration was present in the crown region was about f = 400; the steep parts of the shell slopes, with their relatively small amplitudes, required higher frequencies. Furthermore, in the case of modes where there was a continuous phase shift through 90° along the surface but no proper node, the powder became useless (while the hand held probe remained of limited useability).

In addition to taking photographs of the visible nodal pattern, notes were taken of observations relevant for the interpretation of the given resonance, e.g., amount of phase shifts, higher harmonics and distortions in the response, approximate meridional positions of the circumferential nodal lines, irregularities of the nodal pattern, and type of response of the lower half shell. Finally, if the given resonant mode was of sufficient cleanliness and of sufficient interest, the modal deflections were measured along a suitable meridian. This was done in particular for the lower frequency modes. The distance detector was moved along its supporting half circular arc, Figure 5, and readings were taken at 5° intervals in ϕ.

The test program did not, however, proceed as routinely as this description would seem to indicate. The unexpected observations already mentioned required a good deal of exploratory effort that is not here reported in detail. We list however, numbers of records taken: 164 spectra, 88 photographs of nodal patterns, 68 modal deflection readings along a meridian, 98 readings of all strain gages. Many of these records were more or less duplications made in order to check repeatability, which was generally good, or effects of minor changes in the excitation, or whether a resonance might have been missed. Only a minority of these records are reproduced in this report.

Instrumentation

Much of the instrumentation that was used in the test program is visible in Figure 4. Figure 6 is a block diagram with all instrumentation items indicated. Details of each item are given in the Appendix to this report.

---

*With respect to the horizontal center plane. Symmetry around the circumference is denoted by axisymmetry.
**A technique described in ref. 6.

FUNDAMENTAL MODE, DISCUSSION AND RESULTS

Descriptive Discussion

The fundamental vibration mode of a structure is usually not much different from a suitable static deflection curve. Owing to this observation, it is usually possible to obtain a good approximation to the fundamental frequency f_0 from static results only, without going into a vibration analysis as such. The only required dynamic relation is the Rayleigh quotient; the minimum property of this quotient enhances the accuracy of the frequency prediction.

A torus shell is particularly well suited for an application of this principle if its wall thickness ratio, h, is sufficiently small, its opening ratio, a, not too large, and its internal pressure, p, not too large in relation to h and a; in other words, if the number k (see below) is sufficiently large (as it is in the case of our model). Consider the torus loaded axially by the axisymmetric system of static forces P acting at the inner and the outer circumferences, Figure 1. The overall shell deflection will be as indicated schematically in Figure 1, but most of the actual shell deformation will occur near the two crowns, in regions the width of which is roughly 4R/k; the remaining parts of the shell, its inner part and its outer part, will deflect as comparatively rigid structures. (In the theoretical limit $k \to \infty$, the only shell deformation is a step deformation at each one of the two crowns.) Now the fundamental vibration mode of this torus shell is of the same axisymmetric-antisymmetric type, with the inner and the outer shell moving in opposite directions and the respective mass forces providing the force system corresponding to the static force system P. Accordingly, one would expect the fundamental mode to resemble the static deflection just described.

An illustration of this is Figure 7, the meridional shapes of axisymmetric vibration modes that were obtained analytically by Liepins (ref. 3). The first antisymmetric mode is the fundamental mode here under discussion. For a = 1.33, the number k is fairly high, k = 6.1, and accordingly the shell deformation is concentrated in a fairly narrow crown region, with inner shell and outer shell keeping their circular meridional shapes. In the case a = 10, where k = 3.1, the width of the crown region has about doubled, and hardly any undeformed inner and outer shell parts are left.

As k increases, the percentage of the total shell mass that forms the almost-rigid inner and outer parts of the shell increases; accordingly, the more closely should the fundamental mode resemble the static (under the load system P) deflection curve.

The static analysis of ref. 1 is called "asymptotic" because it becomes asymptotically correct as $k \to \infty$; it again involves simplifications which are better justified with increasing values of k. This asymptotic analysis predicts that the vertical part of the static shell deflection has the form $a \cdot c(\xi k) + b$ with a and b constants, and the function $c(\xi k)$ given by

$$c(x) = \int_0^x \left[1 - \bar{x}\, T_1(\bar{x}) \right] d\bar{x} \tag{1}$$

The coordinate $\xi = \sin \phi$ extends from $\xi = -1$ at the inner circumference to $\xi = +1$ at the outer circumference; $\xi = 0$ at the crowns (Figure 1). The function $T_1(x)$ is the basic antisymmetric solution of the asymptotic torus shell equation. (It follows that $c(x)$ is also an odd function of x.)

According to Eq (1), the number k is simply a scaling factor; the function $c(x)$ does not itself depend directly upon k. (To be exact, the functions $T_1(x)$ and $c(x)$ depend slightly upon the transition parameter ρ^*, see below. However, this dependency is negligible in the present context.)

Let $\overline{w}_0$ be the vertical deflection part of the fundamental vibration mode. From the above, it follows that $\overline{w}_0$ should closely resemble $c(x)$ if k is sufficiently large. As reported in ref. 4, this expectation was excellently confirmed by comparing detailed numerical results of the two analyses, refs. 1 and 3. Also, it was shown in ref. 4 that insertion of results of the asymptotic static analysis into the Rayleigh quotient led to good agreement, over a wide range of shell parameters, with fundamental vibration frequencies predicted by the vibration analysis of ref. 3 . Here we describe the application of the same (quasi-static asymptotic) procedure to the test conditions of our torus model and compare the analytical results with the test results.

<center>Determination of k</center>

The shell parameters are combined in the two numbers A and B. Of these,

$$A = \epsilon_0 \, a^2 = \frac{p}{Eh} \, a^2 \qquad\qquad (\epsilon_0 \text{ is the prestress parameter}) \qquad (2)$$

represents the pressure stiffness, while

$$B = \frac{(a \, h)^2}{12 \, (1 - \nu^2)} \qquad\qquad (3)$$

represents the bending stiffness. In the case $A = 0$ (the unpressurized torus) the scaling relation is $k^6 \sim 1/B$; in the other limit, $B = 0$, the pressurized membrane torus, $k^4 \sim 1/A$. In order to give k a unified mechanical meaning, independent of the relative magnitude of A and B, a normalization of the basic solution of the shell equation is introduced (ref. 1). This leads to

$$k = \frac{n(\rho^*)}{(A^{3/2} + 4B)^{1/6}} \qquad\qquad (4)$$

with ρ^* being the "transition parameter"

$$\rho^* = \frac{A}{(A^{3/2} + 4B)^{2/3}} \tag{5}$$

The function $n(\rho^*)$ is given in Figure 8[†].

The numerical values for ρ^* and k that arise from these relations with the average parameter values for our model, Table I, and the test values for the pressure p are given in Table II.

Deflections

For those test pressures p for which static test data are available (ref. 1) the stiffness S of the model with respect to the static load system P (Figure 1) is given in Table II. This stiffness is more than doubled when p = 15. The relative role of the pressure stiffness is even more pronounced than S would indicate because the contribution of the bending stiffness to S is not constant but decreases as p increases[††]. The point where the two stiffnesses play equivalent roles--the middle of the transition range which to a degree is a matter of definition--is reached already when $p \approx 6.3$, $\rho^* \approx .25$, or slightly higher. When p = 15, the pressure stiffness definitely predominates, which means that the shell behaves much like a membrane.

In Figures 9a and 9b, the measured modal deflections in the fundamental vibration mode are related to the analytical function c(x). The deflections $w_0(\phi)$ normal to the shell were measured, and the numbers

$$\tilde{w}_0(x) \equiv \tilde{w}_0(k \sin\phi) = C_0 \frac{w_0(\phi)}{\cos\phi} + C_1 \tag{6}$$

are plotted, with constants C_0 and C_1 determined for each test condition to fit the flat parts of the analytical curve, away from the crown x = 0. In this manner, a direct comparison between predicted and measured crown deformations is obtained.

Both for the "free" model, Figure 9a, and the "fixed" model, with and without hub weight, Figure 9b, the agreement is entirely satisfactory. There is a slight shift of the experimental points to the right in all cases, indicating that the effective crown point of the model is slightly outside the nominal crown; this was already observed in the static tests with this model (ref. 1, Figure 12). Apart from this shift, the agreement between simplified (asymptotic) analysis and tests is well within testing accuracy for all test conditions and, in particular, for all pressures.

Note that curves drawn through the test points in Figure 9 would have different slopes, due to the increase of the stiffness S with p, if these points were plotted over $\sin\phi$; the scaling factor k serves to make all slopes equal. Also, the wall thickness of the model is increased by 50% to the left of $x \approx -3.5$ (depending upon k) in Figure 9, while the asymptotic analysis assumes a shell of uniform wall thickness. No effect of this discrepancy is apparent in Figure 9.

[†] In the notation of ref. 1

$$n(\rho^*) = (\overline{A}^{3/2} + 4\overline{B})^{1/6}$$

[††] See, e.g., ref. 1 Eq (38)

Frequencies

Analytical predictions for the fundamental frequency f_0 were calculated by means of the Rayleigh quotient

$$f_0^2 = \frac{S}{4\pi^2 M_{eff}} \tag{7}$$

where the effective mass M_{eff} is the integral over all mass points, multiplied with the square of their relative amplitudes.

We considered only vertical amplitudes $\overline{w}_0$ in our analysis. We had to have unit relative amplitude between inner and outer torus circumference; thus

$$2\,\overline{w}_0\,(\xi) = \frac{c(\xi k)}{c(k)} - \delta \tag{8}$$

with δ a constant depending upon the configuration tested. The model mass we allocated to a uniform wall thickness torus, for which

$$dM = \widetilde{M} \cdot \frac{a + \xi}{\sqrt{1 - \xi^2}}\,d\xi; \qquad \widetilde{M} = 4\pi\,h\,R^2\rho \qquad (\rho = \text{mass density}) \tag{9}$$

and to two concentrated mass rings, M^+ and M^-, along outer and inner circumference, respectively. This led to

$$4\,M_{eff} = (1 - \delta)^2 M^+ + (1 + \delta)^2 M^- + \left\{ a\left[\pi\left(1 + \delta^2\right) - F\right] - 4\,\delta\,(1 - G) \right\}\widetilde{M} \tag{10}$$

where

$$F = F(k) = \frac{2}{c^2(k)} \int_0^1 \frac{c^2(k) - c^2(k\xi)}{\sqrt{1 - \xi^2}}\,d\xi$$

$$G = G(k) = \frac{1}{c(k)} \int_0^1 \frac{c(k) - c(k\xi)}{\sqrt{1 - \xi^2}}\,\xi\,d\xi$$

The constant δ is determined by the equilibrium condition of the moving masses

$$\delta = \frac{M^+ - M^- + 2\,\widetilde{M}\,(1 - G)}{M^+ + M^- + a\,\pi\,\widetilde{M}}$$

in the "free" case, while $\delta = 1$ in the "fixed" case.

The mass values that we used are given next in terms of lb weight (mass times g; 1 lb = 454 gram)

	$a\pi\tilde{M}$	M^+	M^-	Total
"free"	46.23	4.17	26.44	76.84
"fixed", no hub weight	46.23	4.17	25.35	75.75
"fixed" with hub weight	46.23	4.17	64.10	114.50

The numbers F and G were calculated to be

p	k	F(k)	G(k)
0	7.38	0.210	0.0012
6	6.96	0.226	0.0018
15	6.50	0.249	0.0023

The frequencies f_0 that resulted are given as $f_{0\text{ calc.}}$ in Table II. The measured frequencies $f_{0\text{ test}}$ are given in the same table, and also the differences

$$\Delta f_0 = f_{0\text{ calc.}} - f_{0\text{ test}} \ .$$

Disregarding the test value for p = 15 in the "free" case, which would appear to be a reading error, all values Δf_0 are positive. One reason is that the horizontal components of the shell vibration have been neglected in our simplified analysis. Another reason is the (slightly) outside position of the effective crown which is indicated by Figure 9. The larger differences in the "fixed" case are presumably due to the fact that the supporting structure was not absolutely rigid, see Figure 12d.

Overall, the agreement between test and simplified analysis is as good as could be expected.

DISCUSSION OF OVERTONE MODES

General

Because the torus shell is flexible in the crown region but relatively rigid away from the crown (as was illustrated by Figure 9), there is a basic difference between the fundamental vibration mode and the overtone modes. In the former, the relatively heavy inner and outer parts of the shell move in opposite directions, with the flexible crown region acting as the connecting spring. Thus a low frequency f_0 results. The overtone modes are either vibrations of the connecting spring alone, with inner and outer shell parts remaining almost undisturbed, or, where (at least) the outer part does take part in the motion, it has to deform and, therefore, its considerable stiffness gets involved. In either case, the expected frequency is considerably higher than the fundamental frequency f_0.

An illustration of this are the axisymmetric vibration modes, Figure 7. Here a = 1.33 corresponds closely to our test model, while the thickness ratio h is almost twice that of our model. The frequency parameter λ is

$$\lambda = \frac{\rho}{E} (2 \pi a R f)^2 \qquad\qquad (11)$$

For the parameter values of our model, Table I ,

$$f = 2030 \sqrt{\lambda} \qquad\qquad (12)$$

Axisymmetric modes we denote by m = 0; in these modes, all nodal lines are circumferential circles. In addition we expect nonaxisymmetric modes, with some number, m, of additional nodal lines that form meridional circles. On a complete circular torus shell, the number of circumferential modes is m/2, and therefore m is always even.

In the case of a cylindrical shell, we would uniquely identify a given mode by two numbers, m and the number, say 2N, of circumferential nodal circles. Figure 7 illustrates several complications that arise in the case of the torus shell. Here N should be the number of zeros along the upper half, say, of the meridional circle. But neither does N always stay constant for a given mode when a is varied (example: third symmetric mode) nor is N always clearly defined. In particular when a = 1.33, disappearance of modal deflection may either indicate a genuine circumferential node or simply disappearance of modal deflection. In a test program it will not always be easy to decide which it is; nor does it matter very much. Figures 15c and d show two sets of measured meridional modal shapes with a good deal of similarly within each set. Some modes have zeros around $\phi = 35°$, others do not. Obviously this is not their major characteristic. In consequence, little use will be made of N in this report.

There are other difficulties that are also, to some extent, already illustrated by the a = 1.33 modes in Fig. 7. The effective suppression, by the rigidity of inner and outer shell parts, of signals between the upper and the lower crown regions has the result that, looking at one crown only, there is often little distinction between symmetric and antisymmetric modes. This effect, seen, for example, in the respective λ values, 0.138 and 0.137, for the two second modes, is more pronounced for thinner shells (e.g., our model). Alternatively, as upper and lower halves of an actual test model are always slightly different, the resonance frequencies of the two half models will not always coincide, and it will therefore be difficult or impossible to identify a given mode as either symmetric or antisymmetric.

A third effect, which again is more pronounced for thinner shells, is that there is a tendency for pairs of modes to form, say a pair of symmetric modes, where the one is almost the mirror shape of the other (ref. 3), reflected at the axis $\xi = 0$. Taking the second and the third effect together, there is thus already for the ideal torus shell a tendency to form clusters of four axisymmetric modes with frequencies close together. In the case of Figure 7, we have three frequencies ($\lambda = 0.130; 0.137; 0.138$) with a total spread of 3%, and the fourth ($\lambda = 0.155$) only 10% off. Adding to this the fact that there will be nonaxisymmetric modes, adding further the expectancy that split modes will form on any actual model, both due to differences between the two half shells and due to deviations from axisymmetry, and considering finally that the air inside the torus model will have its own pneumatic vibration modes, see below, we come to the conclusion that there will be a rather crowded vibration spectrum, the details of which will be difficult to identify. Our test results confirmed this.

Liepins' Frequency Results

Figure 10 is a graphical correlation, in the prestress (ϵ_0) versus wall thickness (h) plane, between all parameter points for which Liepins (ref. 3) gives analytical results and the parameter points which correspond to our test conditions. The first three symmetric and the first three antisymmetric frequencies have been determined from Liepins' λ values for a = 1.33 by means of Eq (12) and are listed in Figure 10 next to the respective parameter points, the former in the left hand box, the latter in the right hand box.

Liepins gives results for m = 0, 2 and 4*, all for a "free" torus shell of uniform wall thickness. Specifically, therefore, Liepins' results for the fundamental mode are not directly applicable to our model with its additional masses; for this reason, a dash rather than a frequency appears for this mode in Figure 10. Indirectly, these specific results are well confirmed; as aforesaid, they agree with the Rayleigh quotient result (ref. 4), and agreement between the latter and our tests was shown in Table II.

Confirmation of Liepins' overtone mode results, Figure 10, is less readily obtainable. To be sure, the additional masses on our model might be expected to play a relatively minor role in these modes; on the other hand, the number of available analytical points is somewhat limited. A proposed interpolation formula (ref. 4, Eq (9)) is limited to axisymmetric modes, and even here it is not quite satisfactory. It starts from the assumption that, for a given mode, the width of the meridional modal shape is proportional to the nominal width 4R/k of the crown region; it was shown to be suitable for interpolation with respect to the opening ratio a but requires refinement for the case that either wall thickness parameter h or pressure parameter ϵ_0 is varied. This situation, and the requirement for an extension to nonaxisymmetric modes, led us to develop the correlation to cylindrical shell vibrations that is discussed in the next section.

Correlation to Cylindrical Shell Vibrations

The classical analysis of the vibration of thin-walled cylindrical shells assumes a system of two types of nodes: meridional circles equally spaced along the cylinder axis, and generatrices equally spaced along the meridian. Thus, the cylindrical shell is divided into equal "retangular" surface elements that are bounded by nodal lines. Each element is assumed to vibrate in a mode that is a sinusoidal half-wave in either direction. This set of assumptions leads to simple boundary conditions for the elements. The analysis is simplified further by assuming the meridional angle $\Delta\phi$ of the element to be so small that shallow shell theory can be applied. The frequency equation that results for the case of a cylindrical shell, prestressed by an internal pressure p, is given in ref. 5. Let $d = R\Delta\phi$ be the meridional arc of the element, and ℓ its axial length. Then

$$4\rho f^2 = \frac{(\pi Rh)^2 E}{12(1-\nu^2)} \left(\frac{1}{d^2} + \frac{1}{\ell^2}\right)^2 + \frac{Ed^4}{(\pi R)^2 (\ell^2 + d^2)^2} + \frac{p}{h} \left(\frac{1}{d^2} + \frac{1}{2\ell^2}\right) \tag{13}$$

The first term on the right is the result of thin plate vibration analysis. The second term represents the stiffening due to curvature, the third term the stiffening due to prestress.

*Liepins (ref. 3) denotes m/2 by n.

We intend to use Eq (13) as a basis for correlating our torus model test results. There are obvious difficulties. The fact that the straight nodal lines of the cylindrical shell are replaced by circumferential circles on the torus is the lesser of these; for a narrow, circular membrane ring, the fundamental frequency is the same as for a rectangular membrane of equal width and length, and it appears reasonable to assume that, given corresponding boundary conditions, a narrow nodal ring along the crown of a torus would be fairly well represented by an equally wide and long nodal strip of a cylindrical shell of equal meridional curvature. More important is that the boundary conditions are different. Away from the crowns, the torus has an additional form stiffness, Figure 9; further, the prestress due to pressure varies along the meridian. Consequently, the nodal spacing will vary along the meridian (compare Figure 7) the modal shape will not be strictly sinusoidal, and, therefore, the boundary conditions will be different and not simple. These reservations we have to keep in mind; on the other hand, Eq (13) is convenient enough to make a comparison worth trying.

At the crowns of a torus shell, the prestress due to p roughly equals the prestress in the corresponding cylinder; thus, Eq (13) can be used directly. Setting $\ell = 2a\pi R/m$ and evaluating Eq (13) for the parameter value of our model and for fixed values of m, the curves drawn in Figures 11a and 11b were obtained. Shown is the frequency f over the elemental angle $\Delta\phi$ given in degrees. Curves for all values of m are drawn for p = 0; a few curves (dashed) are drawn for p = 15.

The most significant observation is that the curves for m ≥ 4 have minima within Figure 11. For m given, the length of the elemental "rectangle" has a given value; if $\Delta\phi$ is small, the first right hand term in Eq (13) is large, that is, on a narrow "rectangle" the plate stiffness predominates. At the minimum of f, the second (curvature) term equals the first (if p = 0); one finds

$$4a\pi Rf_{min} = m\,(Eh/\rho)^{1/2}\left[3\,(1 - \nu^2)\right]^{-1/4} \qquad (p = 0) \qquad (13a)$$

The positions of all minima are shown in Figure 11 for p = 0, 6 and 15. They form a band across Figure 11, and it can be seen that the test points that are also plotted in Figure 11 tend to lie along this band. Intuitively, there is a good reason for this. Assume m given, and vibrate the shell at a given frequency f. This will determine sequences of nodal rings, starting at the inner and the outer circumferences, with the width of each ring determined by its local stiffness parameters. It will be easiest for these sequences to fit together at the crowns if f is at its minimum, that is, if the $\Delta\phi$ of the crown strip can be varied without varying f.

This intuitive explanation does not, of course, establish a necessary condition for a resonance to occur. Also, if $\Delta\phi$ is small enough (m large according to Figure 11) there will not be more or less a single wave at the crown but several waves and accordingly several circumferential nodal rings, see the last photographs in Figure 16. As each one of these rings has its own minimum frequency, the shell resonance frequency f will have to be somewhat higher than f_{min}. An experimental confirmation is the list that follows.

m	p = 0	p = 6	p = 15	
12	702 (49)	754 (52)	823 (42)	
14	820 (36)	871 (70)	940 (—)	f_{min} (13b)
16	937 (53)	987 (—)	1055 (50)	$(f_{test} - f_{min})$
18	1054 (—)	1104 (—)	1173 (48)	

13

Listed are f_{min} and, by means of the differences given in brackets, the lowest resonance frequency having a mode with the given value of m that we observed in our tests*. A dash means: no resonance observed (it should be stressed that the test observations had been made without the benefit of the analytical results). The list clearly indicates that the correlation principle used is basically sound: all differences are positive, and their magnitude is reasonably uniform.

PNEUMATIC RESONANCES

It had been realized while the test program was being planned that the acoustic wavelength of air would be, in the frequency range of interest, of the order of the model dimensions. The pressure transducer, connected with the inside of the model, had been provided accordingly; however, this was done out of curosity rather than because interference of pneumatic occurrences with the shell mechanical vibrations was expected**. Accordingly, a single transducer was installed at the most conveniently available location. A set of transducers, installed directly in the shell wall rather than alongside the pressurization tube, would have been a better tool for positive identification of pneumatic occurrences. Nevertheless, valuable indications were obtained with the installation as it was.

In the description of observed pneumatic resonances that follows, the acoustics of the air inside a rigid infinite cylinder are used as an interpretation guide.

With horizontal excitation ($\phi = 90°$) a model resonance was observed at f = 140 which turned out to be vibratory horizontal translation, with only very little shell deformation. There was no structural spring available as an explanation for this occurrence. The pressure transducer record, Figure 12a-1, exhibited a distinct narrow spike at this frequency. Corresponding spikes occurred at f = 420 = 3 x 140 and at f = 695 ≈ 5 x 140.

Taking c, the speed of sound in air, at its average value***, Table I, and using the mean model circumference $2\pi aR$ as the wavelength, we arrived at f = 138. (The experimental readings varied between f = 139 and f = 142. Shaker location may have played a role. With p = 15, the slightly higher frequency f = 143 was read.)

Everything indicated that the missing spring stiffness was being supplied by a pneumatic resonance, an acoustic vibration in circumferential direction of the inside

---

*"Fixed" test condition. In the "free" condition, the tests had not been extended to sufficiently high frequencies.

**No such effects are reported in ref. 5. On the other hand, Runyan et al., ref. 7, report analysis and tests concerning coupled mechanical-pneumatic longitudinal vibrations of a thin walled cylindrical shell, fixed at one end and provided with a heavy bulkhead at the other end.

***The testing laboratory was air conditioned. It had not been thought necessary to record the air temperature at a given test. Temperature variations will have occurred, in particular, when the model was pressurized or depressurized.

air, with m = 2, and the higher frequency spikes indicating resonances at m = 6 and m = 10, respectively*. To prove the point, part of the air inside the model was replaced by helium. The model resonance at f = 140 disappeared as predicted.

Pure helium would have about tripled the pneumatic resonance frequencies. The pressure record obtained with the helium-air mixture is shown in Figure 12a-2. The m = 2 and m = 6 spikes now appear at f = 253 and f = 761, respectively.

In the m = 2 pneumatic mode, which presumably has nodes at and opposite the shaker, the center of mass of the air moves (mass of air inside model ≈ mass of model/43) and mass equilibrium requires an opposite movement of the model. The air mass center remains stationary if m takes higher values; accordingly no model displacement spikes appear in Figures 12a-3 and 12a-4 at the frequencies of the respective spikes in Figures 12a-1 and 12a-2. (There is also no model displacement spike at m = 2 (f = 253) in Figure 12a-4, perhaps because of the reduced mass of the inside gas.)

The displacements recorded in Figures 12a-3 and 12a-4 are those opposite the shaker ($\theta = 225°$). The sparseness of resonances indicates, as mentioned before, that the horizontal shaker arrangement was not very effective in exciting many model modes. One sees the first genuine overtone shell mode around f = 180 in both records, and again activity in the f = 600 to 700 range. Here are, in the case of air, a number of spikes in the pressure record, Figure 12a-1, which in the case of helium plus air, Figure 12a-2, have contracted to one. The respective displacement records, Figures 12a-3 and 12a-4, are little affected by this but show noticeable differences, caused by the difference in the filling gases, in the range of higher frequencies.

The inside air, apart from being able to vibrate circumferentially, can vibrate in the meridional plane. Acoustic theory predicts modes of the form

$$\text{radial air speed} \sim \cos n(\phi - \phi_0) \cdot J_n'(2\pi f y/c) \tag{14}$$

where y is the meridional radius. At the shell, y = R, the Bessel function derivative has to have a zero. This determines the resonance frequencies. The zero with the smallest argument that is not itself zero occurs with n = 1 and leads to

$$2\pi f R = 1.841 \, c \tag{15}$$

and thus to f = 346.

Set $\phi_0 = 0$. The n = 1 pneumatic resonance then corresponds to vertical translatory vibration of the model as a whole. This model resonance was not found with shaking at the crown (presumably because of the large rocking moment of the shaker force) but was obtained with the shaker at $\phi = 9°$. Figures 12b-1 and 12b-2 show pressure record and displacement record, respectively; the measured frequency was f = 344 (slightly smaller in other tests; f = 347 for p = 15).

Figure 15b shows the modal displacement that was measured along a meridian at f = 344. At this higher frequency, the model is no longer as rigid as it was at f = 140. The modal line has a wave in the crown region, but this wave is displaced from the zero line, so much so that it does not cross this line. There are, thus, no nodes;

*It is not clear why no spikes indicating m = 4,8 and 12 modes appear in Figures 12a-1 and 12a-2.

none would appear in a powder test, Figure 4. An occurrence of this type obviously contradicts the assumptions that we made above in our attempt to correlate toroidal and cylindrical shell vibrations. In particular, equilibrium is impossible without the addition of a vibrating pressure force. The meridional pneumatic resonance mode provides the explanation. Indeed, the observed shell mode was of the $m = 0$ type ($m = 0$ is assumed in the acoustic relation Eq (14)).

Figure 15b also shows a similar occurrence at a much higher frequency, $f = 886$. Apart from the purely circumferential and the purely meridional modes, there will be coupled pneumatic modes. Not having available the appropriate acoustic solution for the toroidal chamber, we estimated the respective resonance frequencies by setting

$$f^2 = (71\ m)^2 + (340\ \bar{n})^2 \tag{16}$$

with $\bar{n} = j'_{ns}/j'_{11}$, and the j' the Bessel function zeros. The purely circumferential resonances arise from Eq (16) with $\bar{n} = 0$, the purely meridional ones with $m = 0$.

The two basic frequencies, $f = 2 \times 71$ and $f = 340$, in Eq (16) were selected for best overall fit with observed pneumatic frequencies. To the modal deflection at $f = 886$ in Figure 15b, where $m = 6$, belongs the following result of Eq (16): $f = 885$ for $m = 6$, $n = 3$. Resonances that are strongly indicated in the pressure records, Figure 12b-1 ($p = 0$) and Figure 12c-1 ($p = 15$), are

m	n	f
0	1	340
2	1	368
6	*	426
2	2	582

The complete lower part of the predicted pneumatic frequency spectrum is shown at the left of Figures 11a and 11b. In all cases where n is given as a number, j' has its first nonzero value for this n; a * for n indicates a purely circumferential mode ($n = 0$, $s = 1$, that is, $\bar{n} = 0$). At frequencies beyond those shown in Figure 11, higher order Bessel function zeros occur, with circular meridional nodal lines of the acoustic mode inside the shell.

Considering the large number of possible pneumatic resonances, the diversity of pressure patterns that they encompass, the fact that ϕ_0 in Eq (14) is a free parameter, there is thus a large multitude of possibilities for structural-pneumatic interactions to occur. To quote from ref. 7: "Structural responses due to acoustic (air) resonances at frequencies considerably different from the structural resonant frequencies are very narrow but still reach peaks close in magnitude to the structural response peak". In consequence, interpretation of vibration tests with closed shell structures becomes involved. As a minimum, one should repeat all tests after putting a different gas inside the shell. In our program this was no longer possible at the time when the importance of pneumatic resonances became evident.

In particular, it would be of interest to explore the effect of a changeover to a different gas on the phase-shifts that were observed. As mentioned before, the phase of the local response amplitude often varied continuously along the model surface between two response peaks, say from 0° to about 180°, with a smaller amplitude at the place of 90° phase shift but with no point of zero amplitude (node) along the path (there were also cases where some relative phase shift between peaks occurred but with a clean node in between). In other words, secondary motions were present. These phase shifts became increasingly pronounced with f increasing and, in particular, with p increasing. Compare with these observations the increase in displacement activity between Figures 12a-3 and 12a-4 (air versus helium) and also the increase in pressure activity between Figures 12c-1 and 12b-1 (p = 15 versus p = 0).

<center>OVERTONE MODES; TEST RESULTS</center>

The test results concerning the fundamental mode were presented earlier in this report. In the discussion of the nature of shell overtone modes and pneumatic modes that followed, some reference has already been made to experimental results. A more complete review, based on the preceding considerations, follows here.

<center>First Overtone Mode</center>

Figure 13 surveys the first three observed resonance frequencies of the "free" model as a function of the internal pressure p. Fundamental mode and m = 2 pneumatic mode have already been discussed. Around f = 200 occurs the first overtone mode, a symmetric m = 2 mode.

From reviewing Figure 10, one would expect the first overtone mode to be an m = 4 mode. Extracting the relation $f^2 \sim h$ for p = 0 from Eq (13a), one would expect a test frequency around f = 160 or f = 180 for this mode. This was not found. On the other hand, Eq (13a) yields f_{min} = 317 for h = 0.01 compared to Liepins result f = 210 for m = 4, and yields f_{min} = 234 for m = 4 and our test condition. This last value agrees well with the actually observed lowest m = 4 modes, see Figure 11a.

In the case of the first overtone mode, records were taken at Δp = 1.5 intervals. Figure 13 exhibits several peculiarities: a split mode, with two distinct frequencies; each frequency does not increase monotonically with p but peaks around p = 7.5.

The meridional nodal line crossed (roughly) from θ = 90° to θ = -90° at the lower frequency, from θ = 0° to θ = 180° at the higher frequency. The meridional modal shapes at the lower frequency and at three pressures p are shown in Figure 14. The corresponding modal shapes of the higher frequency split mode, not shown, were similar, except for some irregularity at p = 0 which disappeared with pressurization.

Figure 14 shows the same three modal shapes twice, in polar and in rectangular coordinates. The polar plot demonstrates some similarity in particular of the p = 0

mode with the first symmetric $m = 0$ mode, Figure 7, at the much larger opening ratio $a = 6.7$. Rectangular coordinates make it easier to compare modal bending curvatures. Test points are shown by symbols at 20° intervals only; test readings were taken at 5° intervals in ϕ, and the curves connect all the test points. The same applies to Figure 15.

In both figures, the overall amplitude of a given measured modal shape is adjusted by applying a suitable factor, so as to achieve some degree of uniformity. The factors are given in the figures.

In the rectangular coordinate plot of Figure 14 the three maxima of deflection amplitude are made equal. The effect of increasing p, and thus of the pressure stiffness, is seen in the widening of the main crown wave and in the disappearance of the secondary wave around $\phi = 20°$.

Resonance requires that the crown wave fits together with the modal deflections of outer and inner shell. It was not possible with our test arrangement to measure the latter beyond $\phi = -55°$. In the polar diagram, an attempt is made to draw (dashed part of the curves) possible modal deflections of this stiffest part of the shell. For $p = 18$, the deflection may have been practically zero, and therein may lie a partial explanation for the drop in resonance frequency.

Curiously, a given mode was the more easily excited the lower its frequency. This is already seen from the factors in Figure 14, and more correctly from the number W that is also given, the relative shaker work input (per cycle) required for equal maximum amplitude, computed taking into account the shell amplitude at the point of excitation.

Clearly, a rigorous vibration analysis will be required to explain such observations quantitatively. The correlation Eq (13) presupposes a sequence of sinusoidal waves with $\Delta\phi$ small and cannot be expected to represent the direct interaction with inner and outer shell that occurs in this low frequency range owing to $\Delta\phi$ being large. Equation (13) gives, for $m = 2$, $f_{min} = 117, 162$ and 204 at $\Delta\phi = 43°$, $48°$ and $53°$ for $p = 0$, 6 and 15, respectively. That for the highest pressure p the measured frequency was below f_{min} is heuristically justified by noting that, as the points of zero curvature of the crown wave were displaced below the zero line (Figure 14), the mass forces were larger, relatively, than Eq (13) assumes.

On the "fixed" model, the first overtone mode was strongly affected by the restraint at $\phi = 90°$. It was distorted: the two meridional nodes were at $\theta = 45°$ and $180°$ on the upper half shell, at $\theta = 0°$ and $225°$ on the lower half shell. There were not, as in the "free" case, two resonances of about equal magnitude. Maximum amplitude frequencies occurred at $f = 169$, 184 and 161 for $p = 0$, 6 and 15, respectively. There were also secondary spikes in this frequency range.

Frequency Spectra

All the spectrum records shown in Figure 12 extend up to $f = 1000$; rms amplitudes are marked in dB, normalized to ± 1 kg shaker force. Figures 12a, b-1 and c-1 have

already been referred to. Figures 12b-2 and 12b-3 compare two shaker positions, off crown ($\phi = 9°$) and at the crown ($\phi = 0°$). Here, as always in Figures 12b and 12c, excitation was applied at the lower half shell, while response signals were taken from the upper half shell (except pressure signals). Both records are crowded but show considerable differences in most details. On the other hand, the strain gage record (strain in meridional direction), Figure 12b-4, has a good deal of similarity with Figure 12b-3, the same shaker position but a different pick-up position. This is as expected. Of course, while the displacement amplitudes decrease in the higher frequency range, the strain amplitudes gain in relative magnitude; this corresponds to the decrease, with f increasing, of the wavelengths of the structural modes.

Figures 12c-1 and 12c-2 correspond to Figures 12b-1 and 12b-2, with now p = 15. As mentioned before, the lower frequency pressure record spikes recur at p = 15, with more activity and higher peaks at higher frequencies. From comparing Figures 12b-2 and 12b-3, one would expect to see more pressure activity in the highest frequency range had excitation been at the crown, at both p = 0 and p = 15, but these records had not been taken. There is, as expected, less agreement regarding frequencies between the two displacement records. However, certain peak activities occur at the same frequency on all four records, e.g., around f = 340 (discussed above in connection with Figure 15b) or around f = 430 (to be discussed below).

The relation between Figures 12c-2 and 12c-3, displacement and strain, respectively, corresponds to that between Figures 12b-3 and 12b-4.

Finally, Figure 12d shows the lateral acceleration, in g, of one of the T-shaped support lugs, visible in Figures 4 and 5, that was supposed to hold the "fixed" model rigidly at its outer circumference. Excitation was applied at the model crown. It is obvious from this record that the support structure, while it was much stiffer than the cylindrical shell carrying a torus-shaped space booster tank would be, nevertheless did not approach the theoretical conditions of rigidity; rather, large coupling effects between model and support structure vibrations did occur. This explains the considerable harmonic distortions that we observed on the "fixed" model.

Spectra of signals taken from the "fixed" model are not shown. These spectra are similarly crowded but are different, in most details, from the spectra taken with the "free" model.

Photographic Records

The photographic records, Figure 16, of nodal patterns made visible by means of semi-sticky powder are identified individually by f, p, model "free" or "fixed" (this is also easily recognized directly from the photographs) and shaker position, at or off the crown. The observed shell mode is interpreted by the number m that is given.

In the photos, $\theta = 0°$ is in front. Little white markers are usually visible in particular at $\theta = \pm 90°$, at $\phi = 0°$, $\pm 20°$, $\pm 40°$...

The lines of white powder that indicate nodal lines are sharp and clear where there is a clean node separating regions of relatively large acceleration amplitude. They are blurred, or disappear altogether, where the node is less clean due to superposition of secondary motion (phase shift) or where the amplitude level is generally small.

The photos are arranged in order of increasing resonance frequency f. They are next referred to in sequence.

$f = 438$. About the lower limit for the powder technique of visualization. Note jagged meridional nodal line at about $\theta = 45°$. Some phase shift and harmonic distortion observed.

$f = 489$. An example of an $m = 0$ mode.

$f = 519$, $m = 6$. Four meridional lines clear, two in back blurred by local phase shift.

$f = 523$. A particularly clean mode, with very little phase shift. Note pair of circumferential nodes at $\phi \approx 20°$ and, more blurred, $\phi \approx 30°$; compare the modal deflection, Figure 15c.

$f = 565$. Corresponds to $f = 523$, but with $p = 15$. Again clean but no double nodal line.

$f = 592$. This is the first of several modes that are denoted by $m = 2$-10. The pair of numbers for m indicates a nonclassical mode: there are in this case ten meridional lines at the inner shell but only two lines at the outer shell (at $\theta = \pm 90°$). The remaining eight inner lines form loops, in pairs, that reach to about $\phi = -20°$. The nodal pattern is quite symmetrical in itself and is arranged symmetrically with respect to the shaker position. Little phase shift observed; nodal lines, in particular also around loops, show proper nodes (zero amplitude).

$f = 606$. Another $m = 2$-10 mode. Here the loops form four distinct almost circular eyes; the next circumferential nodal line, between $\phi = 0°$ and $\phi = -20°$, is distorted into almost a hexagon. Ten inner nodal lines are seen to have equal distances between them below the $\phi \approx -45°$ node.

$f = 610$. The four eyes, less circular here than in the preceding photo, reach almost to $\phi = 0°$. The two frequencies, $f = 610$ and $f = 606$, are quite close together. The displacement spectrum, Figure 12b-3 (same shaker position as in both photos) shows a single narrow spike at $f = 610$, no activity at $f = 606$. The explanation would appear to be that the two photos were records of one and the same mode, taken on different days; that, while the principal characteristic of the mode, the appearance of four eyes, is reproducible, the meridional position of the eyes is not firmly fixed. In fact, an intermediate position of the eyes was observed with this mode on a third day. Also, the amount of phase shift that was observed on this mode did vary somewhat between different days, from "undetectable" to "slight".

Intuitively, it appears well believable that small causes should be able to change the position of the eyes. Such a cause might be a change in the temperature, and thus in the wave speed, of the air inside the model. The pressure record, Figure 12b-1, shows a distinct, though relatively small, spike at $f = 610$. This spike does not correspond to any one of the pneumatic resonances that are predicted by Eq (16).

$f = 612$. A clean $m = 8$ mode on the "fixed" model.

$f = 644$. Another $m = 2$-10 mode, with more phase shift. Outer meridional nodal lines, $\theta = \pm 90°$, had relatively large secondary motion.

f = 660. Preceding comments apply (note pneumatic activity in this f range, Figure 12b-1).

f = 676. An unsymmetrical nodal pattern that we interpret as a distortion of an m = 0-10 mode. In the recorded mode, a pair of meridional nodal lines, those at $\theta = \pm 18°$, get through to the outer shell; outside this narrow range, however, the outer shell vibrates in an m = 0 mode.

f = 705. Generally sharp lines, but interrupted by local secondary motions.

f = 775. Two photos at the same frequency, p = 6 and p = 15. The first, m = 6, fairly clean, in spite of local interruptions that are visible. The second, m = 10, with considerable phase shift outside.

f = 856. We have reached the range of high frequencies where the modes that came out clean enough to be recorded were usually of this type. $\Delta\phi$ observed corresponds closely to its value for minimum f in Eq (13). Refer to the list near the end of the section on correlation to cylindrical shell vibrations.

f = 862. Same as preceding, except "free" model. Slightly higher f, more secondary motion.

f = 990 (p = 0) and f = 1106 (p = 15). Correspond closely to each other. Similarity of irregularities in a number of shell surface locations.

f = 1211. Highest resonance frequency for which a photographic record was taken.

Remark on Nonclassical Modes

Possible causes for the appearance, in vibration tests with thin-walled cylindrical and conical shells, of nonclassical modes (here generally modes that do not allow separation of variables) have been the subject of discussions in the literature. Recent contributions are those of Koval (ref. 6) and Mixson (ref. 8). Causes considered include: the fact that the shaker input is localized in such tests; superposition of natural modes having closely spaced frequencies. In particular, if a model imperfection causes a split mode, with different node locations at the two frequencies (example: the first overtone mode of our model) then the superposition of the two modes that occurs in the intermediate frequency range can lead to "exotic nodal patterns" (ref. 6).

The thinner the shell, the more likely this is to occur. In Koval's tests (ref. 6), h = 0.0033, the cylindrical shell had a lap joint, an obvious cause for split modes. In Mixson's tests (ref. 8), conical frustrum shells, all mixed modes were eliminated by proper shaker positioning on the two shells, h = 0.0029 (based on mean radius) and h = 0.0015, that had clean butt welds. One nonclassical mode was observed with another shell, h = 0.0015, that had a lap joint, and numerous such modes were observed with the thinnest shell, h = 0.0008, which had both lap joints and local wrinkles.

Our own torus shell model, h = 0.0055, had butt welds, with all excess material removed on the outside and little excess material at the inside. The model was well manufactured (though not perfect, as is demonstrated by the fact that the first overtone mode was split). All observations pointed to the conclusions that the observed

nonclassical modes were genuine natural modes and that such modes are an inherent property of the torus shell configuration. Compare the discussion of the f = 610 mode in the preceding section. There was a nodal pattern of high regularity, relatively free from secondary motion, not affected by variation of the shaker position. There was a clean spike in the displacement spectrum record. Also, the same characteristic, many more meridional nodes on the inner shell than on the outer shell, appeared at a number of frequencies.

It should perhaps be stressed that the nodal pattern that was indicated by the powder lines was verified in detail. Everywhere the phase shifted over to its opposite on crossing a nodal line (one checks readily that the pattern does indeed allow one to allocate either + or - to each surface element in such a manner that a changeover occurs at each nodal line). On the other hand, the phase did not change, for example, between $\theta = + 90°$ and $\theta = -90°$ along the circumferential strip, f = 606 in Figure 16, that is bordered by the hexagonal nodal line outside and is narrowed locally by the eyes inside; nor did the phase change along the corresponding, but even narrower (at the eyes) strip in the case f = 610.

All the loops that we observed were positioned on the inner shell, in the range of negative Gaussian curvature. This may be significant. In a way it is unexpected: the hub of a torus shell is its stiffest part (already in the case of uniform wall thickness, and even more so if, as on our model, the shell is strengthened here). Apart from this, there is more area on the outer shell, and one would rather expect additional meridional nodes to form there (in the tests ref. 8 with conical frustrum shells all additional nodes formed at the wider end).

We have, of course, to consider the possibility that any one m = 2-10 mode, say, might have been a mixed mode, a superposition of two classical modes; in this case, of an m = 2 mode and an m = 10 mode, the two modes having the same resonance frequency, and both having nodes at $\theta = \pm90°$. Figure 17 describes the types of nodal configurations that would arise from such a superposition, both in the neighborhood of a circumferential node of the m = 2 mode (A = 0) and of the m = 10 mode (B = 0). Attempting to reconcile Figure 17 with any one of the m = 2-10 modes of Figure 16, one comes to the conclusion that this requires an m = 2 mode having essentially zero amplitude inside the loops, combined with an m = 10 mode having essentially zero amplitude outside the crown. A slight tendency for larger amplitudes inside than outside may be inferred from Figures 14 to 16, see in particular the m = 10, p = 0 mode Figure 16, f = 705. There is thus a certain, though not convincing, tendency toward the existence of the required m = 10 mode; the same argument makes the required m = 2 mode an even more unlikely occurrence.

The final judgement has to come from a more detailed experimental and also an analytical investigation. Regarding the former, here is the place to add a remark on shaker effects. Mixson, ref. 8, shows remarkably large (and not fully explained) effects (frequency changes) due to changing over to an air jet shaker. While for completeness a similar comparison should be made on the torus shell, no serious effects are here expected: Mixson used his thinnest model (h = 0.008) and excited directly at the observed mode, while in our "free" tests, with our much sturdier model, excitation occurred at the lower half shell.

Apart from m = 2-10 modes, we observed one 4-12 mode (with f = 695, see Figure 11a). Furthermore, Figure 16, f = 676, would seem to indicate that a complete m = 0-10 mode is possible in principle.

Modal Deflections

Some of the records of meridional modal shapes, Figures 14 and 15, have already been referred to in the discussions of pneumatic resonances and of the first overtone mode, and the manner of presentation has been explained there. Brief remarks on the remaining records are here added.

Figure 15a compares two m = 4 modes at widely different frequencies. At the higher frequency, there are more waves, and in consequence $\Delta\phi$ is smaller; approximation of each half-wave by a sine-curve is more appropriate in that the points of zero bending curvature coincide better with the nodes (zeros). The overall displacement amplitude is much reduced at the higher frequency.

Figure 15c shows three examples (one mode for each p) of the set of modes that was observed around f = 520. These samples, in particular the curve for p = 15 with its two closely spaced nodes at ϕ = 22° and 35° (compare Figure 16) illustrate again that, in applying Eq (13), one should perhaps define $\Delta\phi$ as the distance of consecutive points of zero modal curvature rather than as the distance between observed nodal lines.

Figure 15d shows four m = 2-10 modal deflections, all measured along the meridian opposite the shaker meridian and therefore between two eyes. A good deal of similarity exists between the four curves. The halfwaves that include the point ϕ = 0° are reasonably well sinusoidal. The fact that the eyes are positioned within the ϕ-range of this halfwave in the case f = 610 but not in the cases f = 592 and f = 644, see Figure 16, does not produce any obvious difference in Figure 15d.

Interpretation of "Free" Model Results

Having commented on the records that were taken during the tests in the preceding sections, we are finally ready to review Figure 11, the attempt to correlate analytical curves, Eq (13), and experimental results.

Of the analytical curves, only a few are drawn for p = 15, and none for p = 6. All minima are shown, however, and are emphasized. Thus the missing curves are readily constructed to the accuracy that is required for the present discussion. To the left are the predicted pneumatic resonances, Eq (16). With each experimental point, m and type of symmetry are indicated whenever this information is available.

The overall impression of Figure 11a, the "free" model correlation, which we are going to discuss first, is that the test points tend to lie in a band across this figure and that this band roughly coincides with the band of minima. There are deviations from this overall impression, a number of test points to the left of the band above f = 600, and a number of test points to the right at f ≈ 440 and f ≈ 520.

Before remarking on these "deviations", we have to emphasize that the $\Delta\phi$-value that has been allocated in Figure 11b to a given observed resonance is somewhat arbitrary in each case. The correlation had not been planned originally, and the tests had not been performed with it in mind. After the test program had been completed, $\Delta\phi$-values, here defined as the average distance between nodal lines near the crown, were estimated on the basis of photographs and of notes on test observations. The modal

deflection readings, Figure 15, were not much relied upon because they were not available for all modes and because some circumferential nodes are not circles (e.g., Figure 16, f = 606). With nodes unequally spaced (e.g., Figure 15c, f = 519) a mean value was taken. In a number of cases, $\Delta\phi$ was estimated to the nearest 5° only, as is evident from Figure 11a. In other cases, the estimate was somewhat more accurate, but none should be taken to be reliable to better than ± 2°.

The observation that the test points tend to lie within the band of minima is not a prediction of Eq (13) but is simply an observation (for which we gave an intuitive explanation). Equation (13) is a tentative prediction that each test point should lie somewhere along its m-curve. Quite often, this prediction is seen to be well fulfilled; in particular, it is reasonably well fulfilled by the test points outside the band of minima to the upper left. On the other hand, there are test points that do lie within the band of minima but do not lie near their m-curve. An example is the f = 697, p = 0, m = 4 test point for which Figure 15a shows the deflection curve. As this point is quite close to another p = 0 point with, however, m = 4-12, one might suspect that the first point might have been, in reality, also an m = 4-12 point. The photographic record (not shown) contradicts this suspicion.

This brings up another problem. A number of m = 2-10 points are seen to lie close enough to their respective m = 10 curves. However, in the crown range, where $\Delta\phi$ was measured, some of these resonances looked rather like perfect m = 2 modes, e.g., Figure 16, f = 592. The conclusion to be drawn from this last observation is that one should examine the nonclassical modes in considerable more detail than was possible within the present program.

We turn now to the deviations to the right, at lower frequencies. First, it is interesting indeed that there were m = 4 modes at about the same frequency, f = 440, at all pressures p, and two each at p = 0 and p = 15. There was in two of these modes so much distortion that m could not be determined with certainty; these points are identified as m = 4(6). Both facts would seem to indicate a pneumatic cause. An m = 4 pneumatic mode is indeed predicted for f = 443; however, the pneumatic activity visible in Figures 12b-1 and 12c-1 corresponds, in its frequency f, better to the pneumatic m = 6 mode at f = 426. There is thus a contradiction. Unfortunately, because of the distortions, the meridional modal shape had not been measured and is not available for examination for pneumatic effects.

Note the sequence of reasonably "legitimate" m = 6 modes, f = 395 for p = 0, f = 440 for p = 6 (distorted) and f = 520 for p = 15. The m = 4 modes around f = 520, again with m = 4, form the second deviation. Here there is no predicted pneumatic m = 4 mode nearby. No pneumatic activity is shown in Figure 12b-1, only slight activity in Figure 12c-1. The meridional deflection shapes, Figure 15c, do not indicate any obvious pneumatic effects either; also, these modes are (relatively) clean. On the other hand, their meridional mode shapes, Figure 15c, are far from being sinusoidal, and it can be argued that their effective $\Delta\phi$ are smaller than the $\Delta\phi$ shown in Figure 11a.

The overall conclusion to be drawn from Figure 11a is that Eq (13) forms a helpful basis for correlating the observed vibration modes; that there are exceptions, as was to be expected; that for unknown reasons multiple exceptions occurred at certain frequencies, independent of the internal pressure p; that in general, however, identifiable vibration modes tended to appear within the band of minima of the analytical curves.

Observed modes that are not shown in Figure 11a because the observed $\Delta\phi$ is outside, to the right, of the range shown in Figure 11a are: the first overtone mode, Figure 14, and several modes that were clearly products of pneumatic activity, namely, m = 0, f ≈ 340 modes that appeared at all pressures p, compare Figure 15b; the f = 886 mode, p = 6, that is also shown in Figure 15b; plus two modes with p = 15, f = 606 and f = 672. (Of the latter, the first, m = 2, may be the predicted pneumatic mode at f = 584; the second was too much distorted for proper identification.) Thus, the number of observed modes with definite pneumatic effects increased with p.

We should also try to correlate the test results with Liepins' analytical prediction, Figure 10. The first identified m = 0 mode in Figure 11a is f = 649 (p=0). With the "fixed" model the lowest m = 0 mode was f = 489 (p=0), Figures 15 and 11b. Both frequencies lie within the range of plausible interpolations in Figure 10. Unfortunately, it would be difficult to make a more precise statement.

Interpretation of "Fixed" Model Results

The test observations with the "fixed" model are shown in Figure 11b. In this earlier test program often only the number, N, of circumferential nodes on the upper shell, not their position, had been noted; thus $\Delta\phi$ is often unknown. These resonances are listed to the right of Figure 11b. The number N is given, but the reservation that was made in the general discussion of overtone modes does apply.

The overall impression of Figure 11b is the same as that of Figure 11a. The details differ, in particular in the lower frequency range. There are fewer modes around f = 440; there is, however, again a set of m = 4 or 6 modes around f = 520. More modes are recorded near the upper frequency limit than in Figure 11a. Partially, this may be due to the fact that, in testing the "free" model, we placed more emphasis on recording details in the lower and medium frequency ranges than on re-recording the upper range, where the quantitative difference was generally small; compare, e.g., Figure 16, f = 856 and f = 862. It seems, however, as shown in the same two photographs, that, while there was usually harmonic distortion with the "fixed" model due to coupling with the support structure, the amount of phase shift, that is, of secondary motion at the excitation frequency, was smaller, and that in consequence mode identification was easier with the "fixed" model.

An explanation of the last point would seem to be that slightly different resonance frequencies of upper and lower shell led to the phase shifts on the "free" model, while vibratory signals between the two shell halves were largely suppressed on the "fixed" model.

CONCLUSIONS

The experimental model of a complete circular torus shell corresponded in its opening ratio to a space booster tank. It was vibration tested in its "free" condition, and in a "fixed" condition where it was supported along its outer circumference. In both conditions, the measured fundamental mode response, both frequency and modal deflection, agreed well with the predictions obtained from static asymptotic analysis by means of the Rayleigh quotient.

The first overtone mode was a split mode; in both its components, the resonance frequency first increased and then decreased as the model was pressurized. The responses, frequency and nodal pattern, at higher resonance frequencies were reasonably well correlated by means of curves derived from cylindrical shell analysis; in particular, it was found that identifiable modes appeared usually within the band of minima of these curves. Intuitively, there is a good reason for this coincidence. There were also interesting exceptions.

Of particular interest were two unexpected occurrences: nonclassical modes and pneumatic effects. In the former, many (usually eight) more meridional modal lines existed on the inner part of the torus than on the outer part. Pairs of the additional nodes formed nodal loops. It appeared that these loops could shift in meridional direction with relative ease, but always stayed within the range of negative Gaussian curvature of the shell.

The other unexpected occurrences were shell vibrations showing large pneumatic effects. Acoustic resonances of the air inside the model were shown to exist by replacing part of the air inside the model by helium. There were circumferential pneumatic modes, transverse pneumatic modes, and combinations. There were corresponding responses of the model as a whole, and modes that were obviously distorted by pneumatic pressures. There were also secondary motions, recognizable as continuous phase shifts in the response along the shell surface, which became increasingly pronounced as the internal pressure was increased.

Not all questions that were posed by these unexpected occurrences could have been resolved within the limitations of the present program, and, in these respects, this program has to be considered as preliminary. In a future program, all testing should be done twice, with two different gases inside the model. Alternative excitation techniques (e.g., air jet shaker) should be tried in order to eliminate possible doubts in this direction. Attention should be concentrated on specific questions, as the detailed topography and the sensitivity of nonclassical modes, and furthermore on closer examination of those modes which, in the present evaluation, seemed to fall outside the band that is formed by most of the resonances.

Martin Company
   Baltimore, Maryland
      December 15, 1966

REFERENCES

1. Jordan, P. F.: Analytical and Experimental Investigation of a Pressurized Toroidal Shell. NASA CR-261, 1965.

2. Liepins, A. A.: Free Vibrations of the Prestressed Toroidal Membrane. AIAA J., vol. 3, no. 11, Nov. 1965, pp. 1924-33.

3. Liepins, A. A.: Flexural Vibrations of the Prestressed Toroidal Shell. NASA CR-296, 1965.

4. Jordan, P. F.: Vibration and Buckling of Pressurized Torus Shells. AIAA Paper No. 66-445 (4th Aerospace Sciences Meeting, June 1966).

5. Fung, Y. C.; Sechler, E. E.; and Kaplan, A.: On the Vibration of Thin Cylindrical Shells Under Internal Pressure. J. Aeron. Sci. vol. 24, no. 9, Sept. 1957, pp. 650-660.

6. Koval, L. R.: Note on the Vibrational Characteristics of Thin-Walled Shells. AIAA J., vol. 4, no. 3, Mar. 1966, pp. 571/2.

7. Runyan, H. L.; Pratt, K. G.; and Pierce, H. B.: Some Hydro-Elastic-Pneumatic Problems Arising in the Structural Dynamics of Launch Vehicles, ASME Paper No. 65-AV-27 (Aviation and Space Conference, March 1965).

8. Mixson, J. S.: On the Modes of Vibration of Conical Frustrum Shells with Free Ends, AIAA Paper No. 66-450 (4th Aerospace Sciences Meeting, June 1966).

APPENDIX

List of Test Instrumentation Items

Electrodynamic Shaker. Ling model LPM-25 with force rating of ±25 lb,* armature weight (including forcing bar) of 0.18 lb, locked armature resonance of 9000 cps, and stiffness of armature carrying flexure (no voltage applied) of 8.5 lb/in.

Power Amplifiers (2). Optimation, Inc. model PA 250 AC.

Distance Detector. Photocon Research, Inc. model PT-5 with 0.25-in. diameter probe.

Hand-Held Probe. Dynamic Devices, Inc. model 101. This is a self-generating velocity type device.

X-Y Plotter. F. L. Mosley model 5S.

Logarithmic Converter. F. L. Mosley model 60B.

Frequency to Voltage Converter. Vidar model 322 with a 2000 cps insert.

Variable Pass Electronic Filter. Spencer-Kennedy Labs model 308A.

Frequency Counter. Beckman Instrument Co. model 554.

Cathode Ray Oscilloscopes (2). One Tektronix model 541A with type 53/54B plug-in unit, and one Hewlett-Packard model 130B.

Audio Frequency Signal Generators (2). (Audio Oscillators). One Hewlett-Packard model 200 and one Hewlett-Packard model 200 CD.

Bridge Balance and Selector Boxes (3). Young Testing Machine Co. These devices were used with the strain gages.

Bridge Balance Box. Manufactured by the Martin Co. and used with the pressure transducer.

D. C. Digital Voltmeter. Electro-Instruments, Inc. model 8409 MB.

A. C. Digital Voltmeter. Electro-Instruments, Inc. model 139 MD.

High Gain Differential Amplifiers (2). Dana Laboratories, Inc. model 2003.

D. C. Power Supply. Power Designs, Inc. model 5005R.

Mercury Manometer. Meriam Instrument Co. model A-338.

-----

*1 lb = 0.454 kg; 1 inch = 2.54 cm; 1 cps = 1 Hz; 1 psi = 0.0703 kg/cm^2.

Pressure Transducer. Consolidated Electrodynamics Corp. model 4-312, having a pressure range of 0 to 50 psia and diaphragm resonance at 9300 cps.

Pressure Regulator. Foxboro Corp. type 20 Airdron Regulator.

Strain Gages (58). Budd Co. model C12-121-R2TC-350.

Frequency Analyzer. Bruel and Kjaer Inc. model 2105.

TABLE I

MODEL PARAMETER VALUES AND NOTATION

Model parameter values used in analyses, obtained by averaging measured values

R	meridional radius	11.5 in. = 29.21 cm
a	opening ratio	1.365 = 1.365
hR	shell wall thickness (uniform part of shell)	0.0627 in. = 1.59 mm
E	Young's modulus	1.07×10^7 lb/in.^{2} = 7.52×10^5 kg/cm^2
ν	Poisson's ratio	0.32 = 0.32

Other quantities used in analyses

$\rho \cdot g$	shell material weight	0.103 lb/in.^{3} = 2.85 kg/dm^3
g	gravity acceleration	386.1 in./sec^2 = 9.807 m/sec^2
c	speed of sound in air	1132 ft/sec = 345 m/sec
	(in pure helium	3312 ft/sec = 1010 m/sec)

Other notation items

f	frequency	1 cps = 1 Hz
p	internal overpressure	1 lb/in.^{2} = 0.0703 kg/cm^2
ϵ_0	reference strain	= p/Eh

TABLE II

FUNDAMENTAL FREQUENCIES

test condition	p (lb/in.^{2})	0	3	6	9	12	15	18
	p (kg/cm^2)	0	0.211	0.422	0.633	0.844	1.055	1.266
	$\rho*$	0	0.124	0.236	0.332	0.415	0.485	0.544
	k	7.38	7.16	6.96	6.79	6.64	6.50	6.36
	S (lb/in.)	4583		7226			10612	
	S (kg/cm)	818		1290			1895	
"free"	$f_{0\,test}$	48.7		61.3			75.8	
	$f_{0\,calc.}$	49.0		61.6			74.9	
	Δf_0	+0.3		+0.3			−0.9	
"fixed" no hubweight	$f_{0\,test}$	33.8	38.2	42.6	46.2	49.2	52.0	54.5
	$f_{0\,calc.}$	34.8		43.8			53.1	
	Δf_0	+1.0		+1.2			+1.1	
"fixed" with hubweight	$f_{0\,test}$	24.1		30.1			37.0	
	$f_{0\,calc.}$	24.3		30.6			37.1	
	Δf_0	+0.2		+0.5			+0.1	
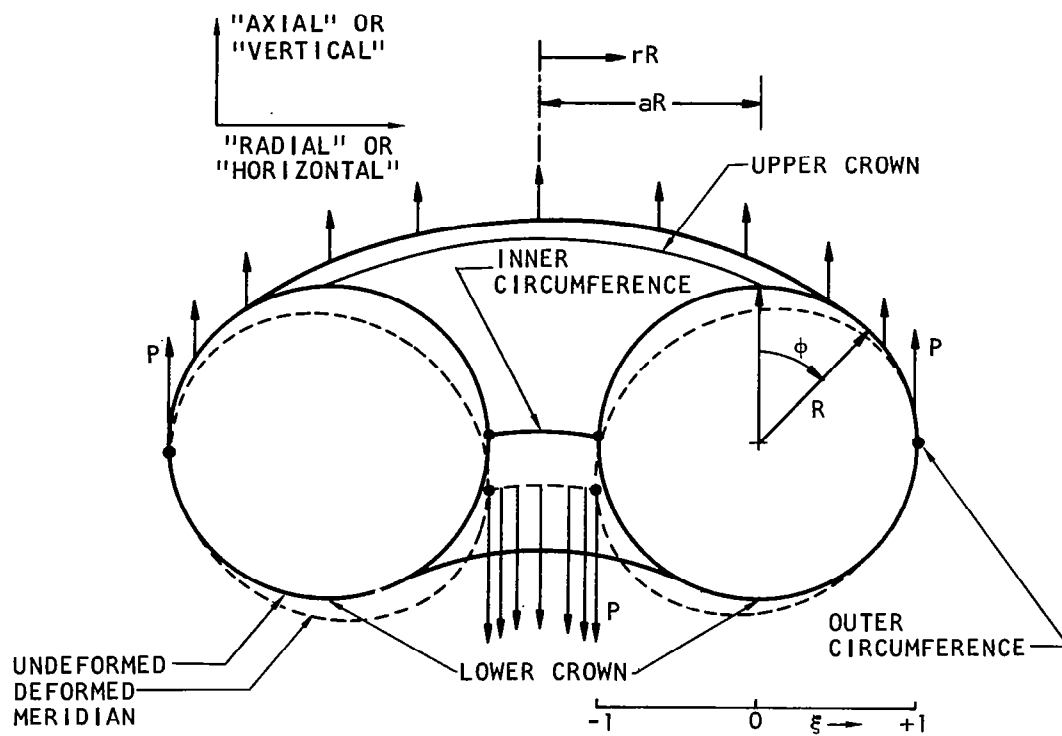
Fig. 1. Circular Torus Shell Under Axial Load P and Notation
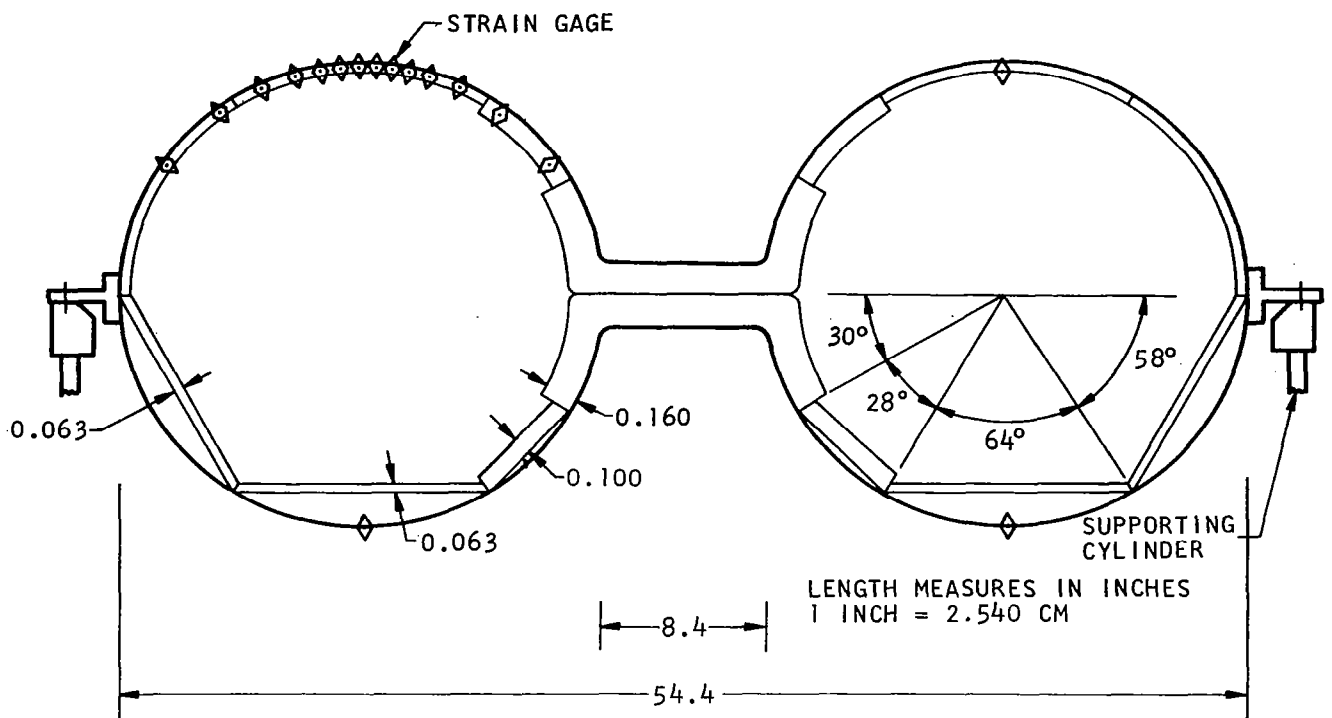
Fig. 2. Experimental Model, Cross Section
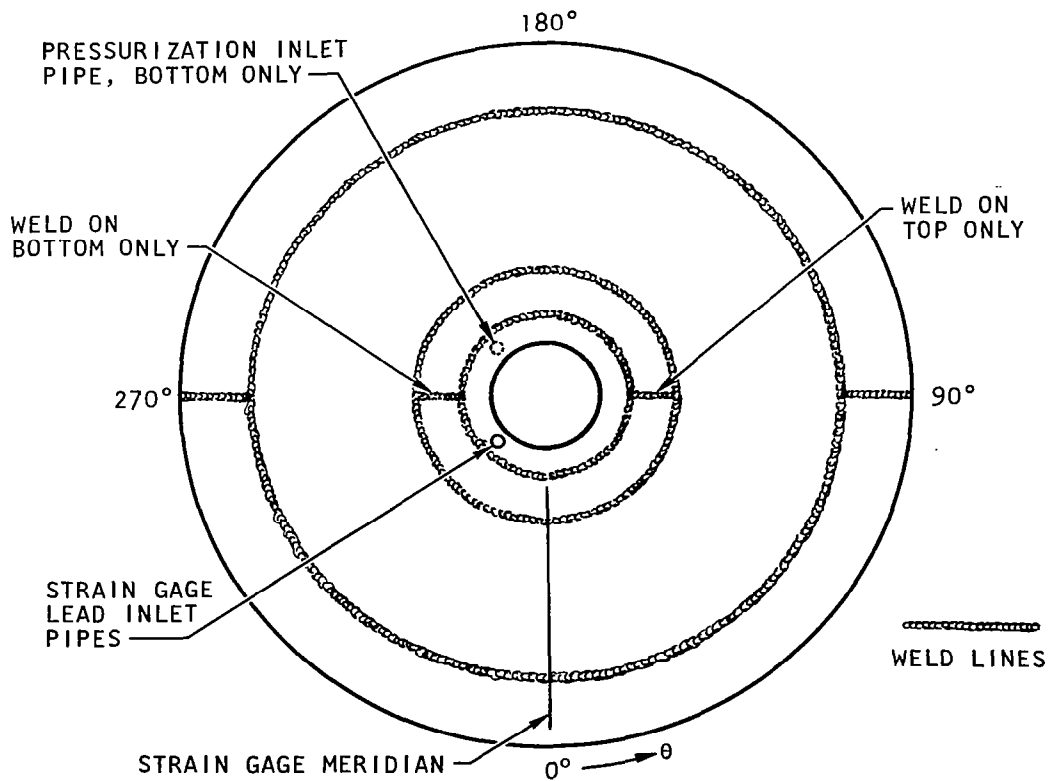
Fig. 3. Top View of Model (schematic)

STRAIN GAGE INSTRUMENTATION

SHAKER POWER AMPLIFIERS

VARIABLE PASS ELECTRONIC FILTER

STRAIN GAGE MERIDIAN

AUDIO OSCILLATOR

X-Y-PLOTTER

LOG CONVERTER

MODEL

AUDIO OSCILLATOR AND DRIVE

MODEL SUPPORT

FREQUENCY COUNTER

OSCILLOSCOPE

DISTANCE DETECTOR BALANCE

SHAKER SUPPORT
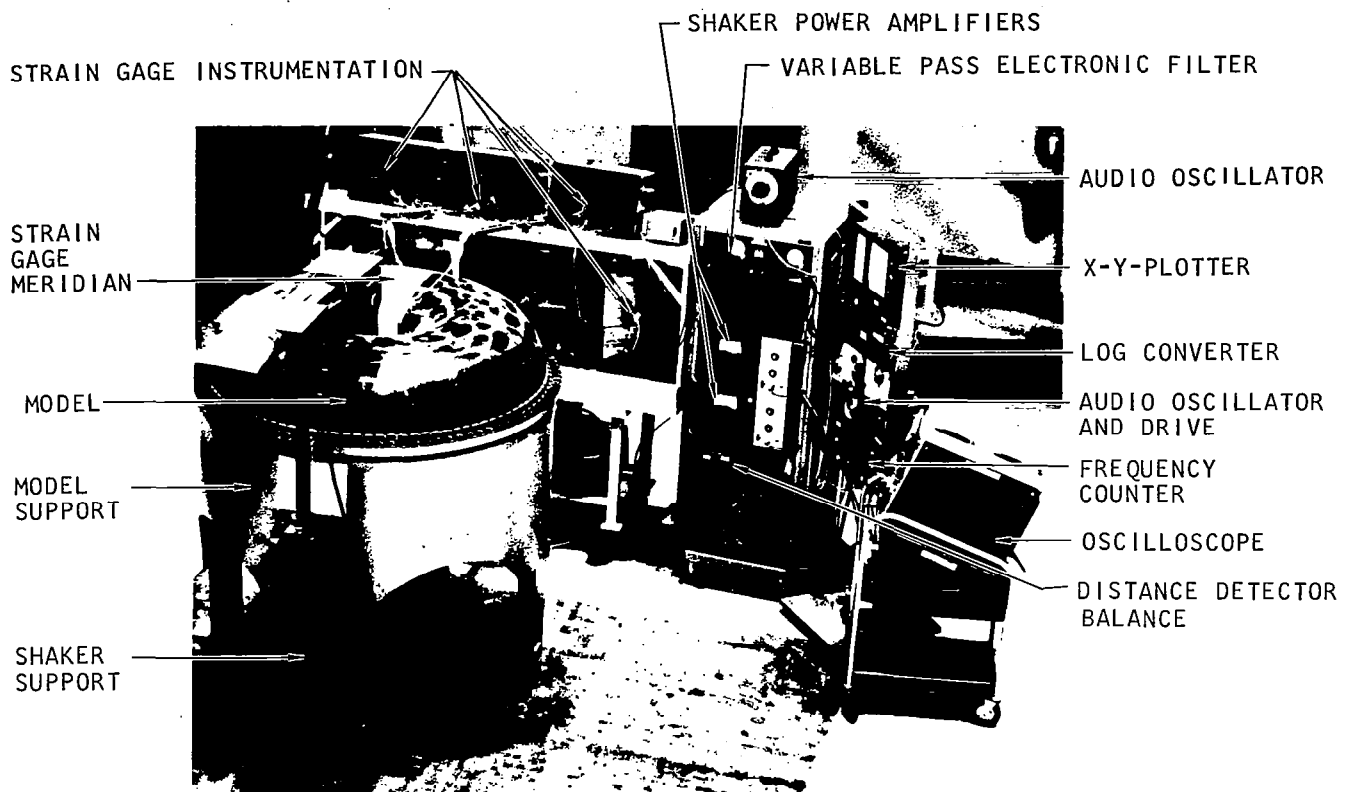
Fig. 4. Test Setup, General Arrangement

DISTANCE DETECTOR

MERIDIAN TRAVERSING SUPPORT ARCH

ELECTRODYNAMIC SHAKER
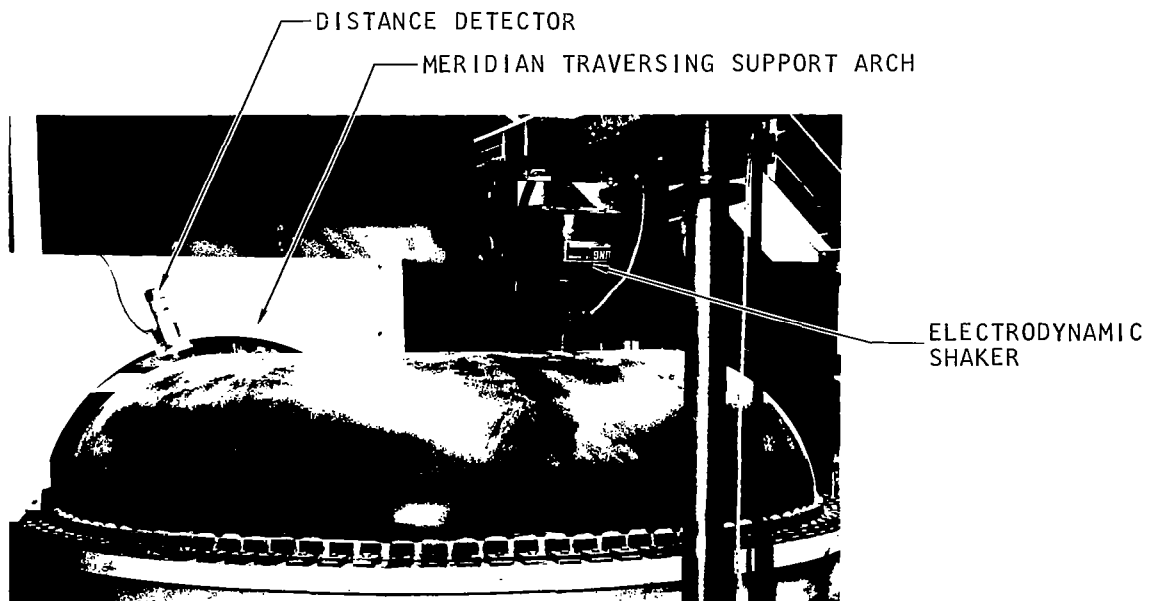
Fig. 5. Shaker and Distance Detector Arrangement
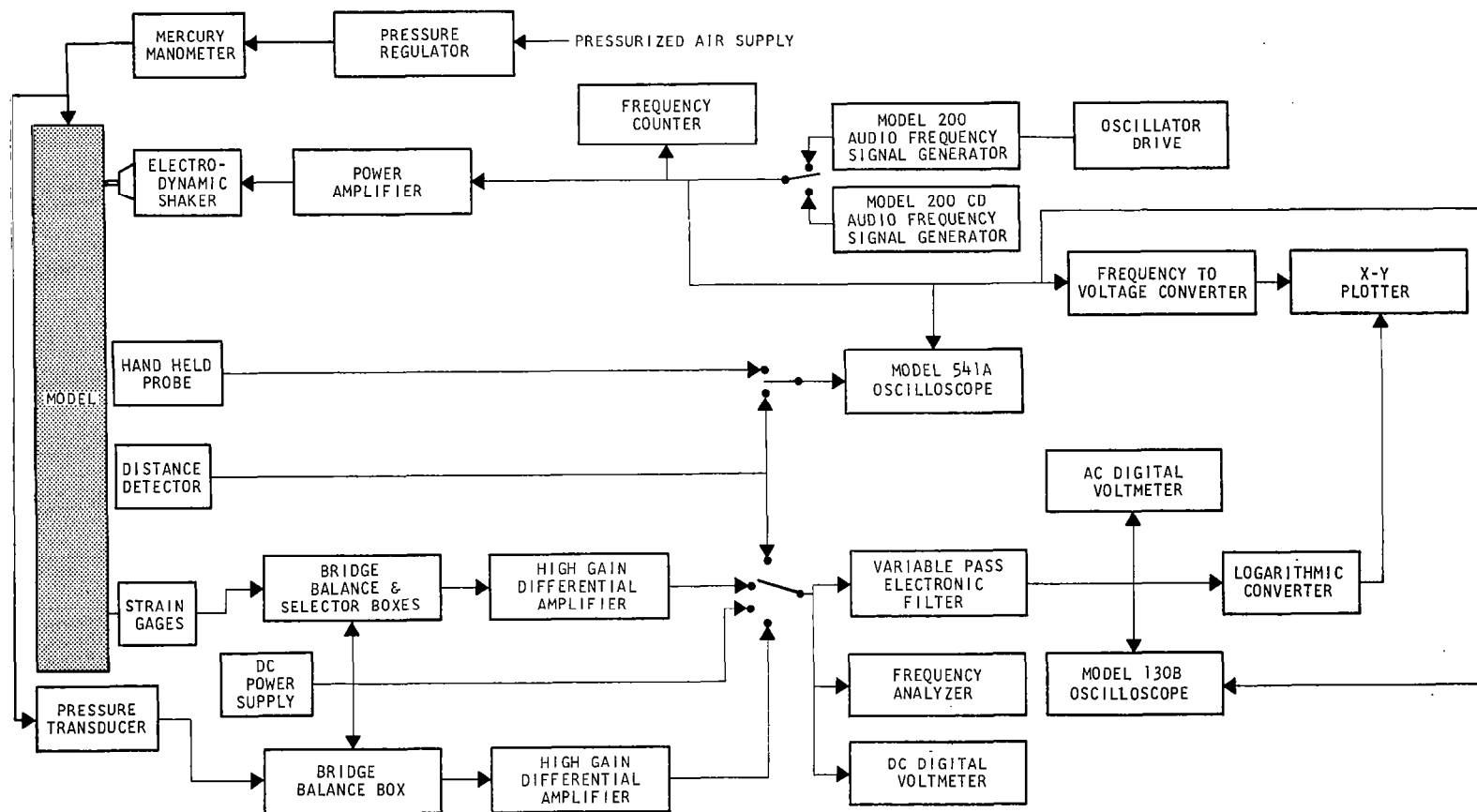
Fig. 6. Instrumentation Block Diagram

FUNDAMENTAL MODE

Symmetric Modes			Antisymmetric Modes	

$a = 6.7$
$\lambda = 0.346$

$a = 1.33$
$\lambda = 0.130$

FIRST

$a = 10$
$\lambda = 0.0145$

$a = 1.33$
$p = 0.00239$

$a = 25$
$\lambda = 0.817$

$a = 1.33$
$\lambda = 0.138$

SECOND

$a = 20$
$\lambda = 0.682$

$a = 1.33$
$\lambda = 0.137$

$a = 20$
$\lambda = 1.008$

$a = 1.33$
$\lambda = 0.199$

THIRD

$a = 13.3$
$\lambda = 0.779$

$a = 1.33$
$\lambda = 0.155$

$a = 16.7$
$\lambda = 1.0615$

$a = 1.33$
$\lambda = 0.248$

FOURTH

$a = 13.3$
$\lambda = 1.037$

$a = 1.33$
$\lambda = 0.239$

Symmetric Modes

Antisymmetric Modes
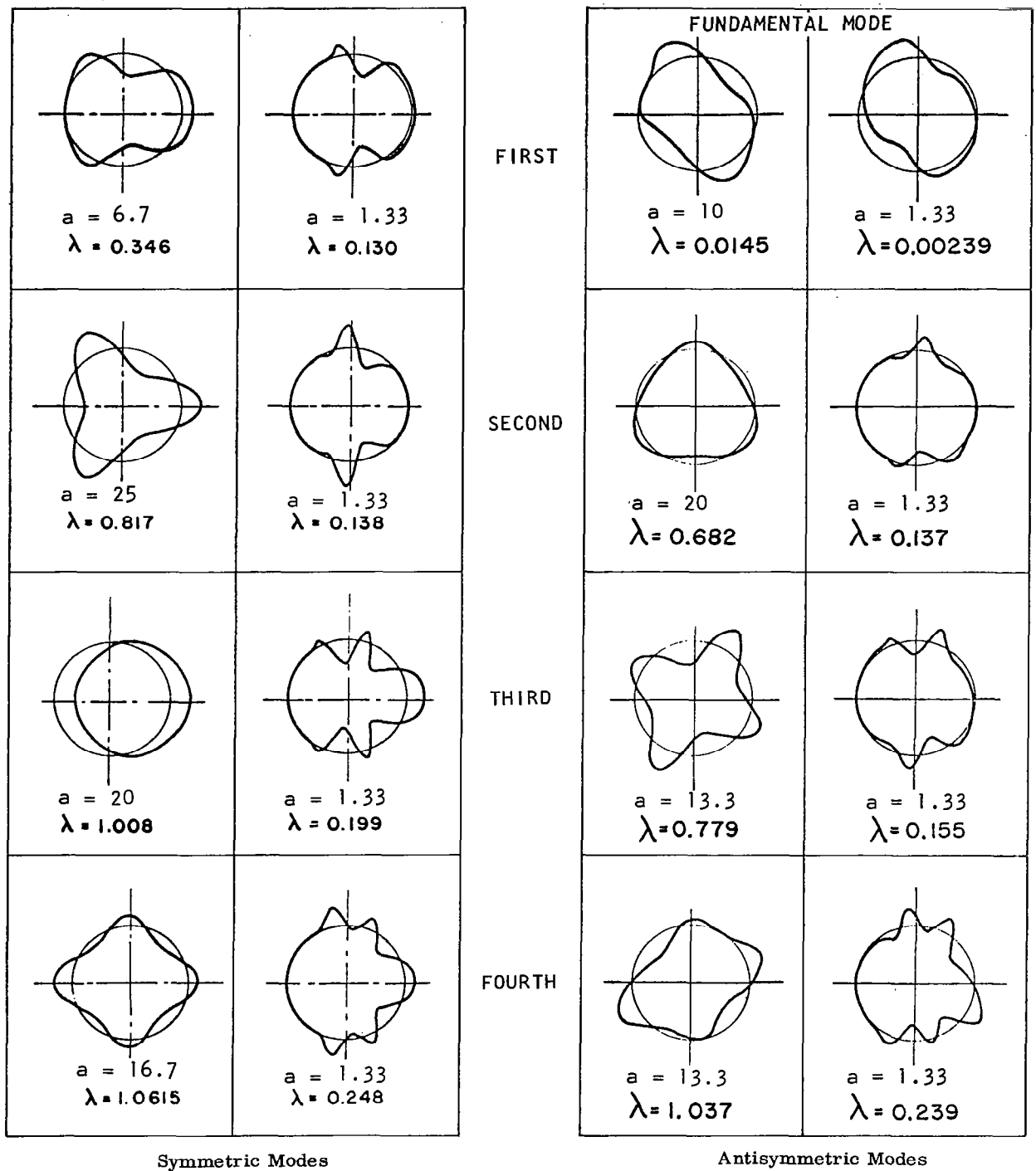
Fig. 7. Meridional Modal Shapes in Axisymmetric Vibration (analytical from Ref. 3) $p = 0$; $h = 0.01$. Axis of rotation to the left.
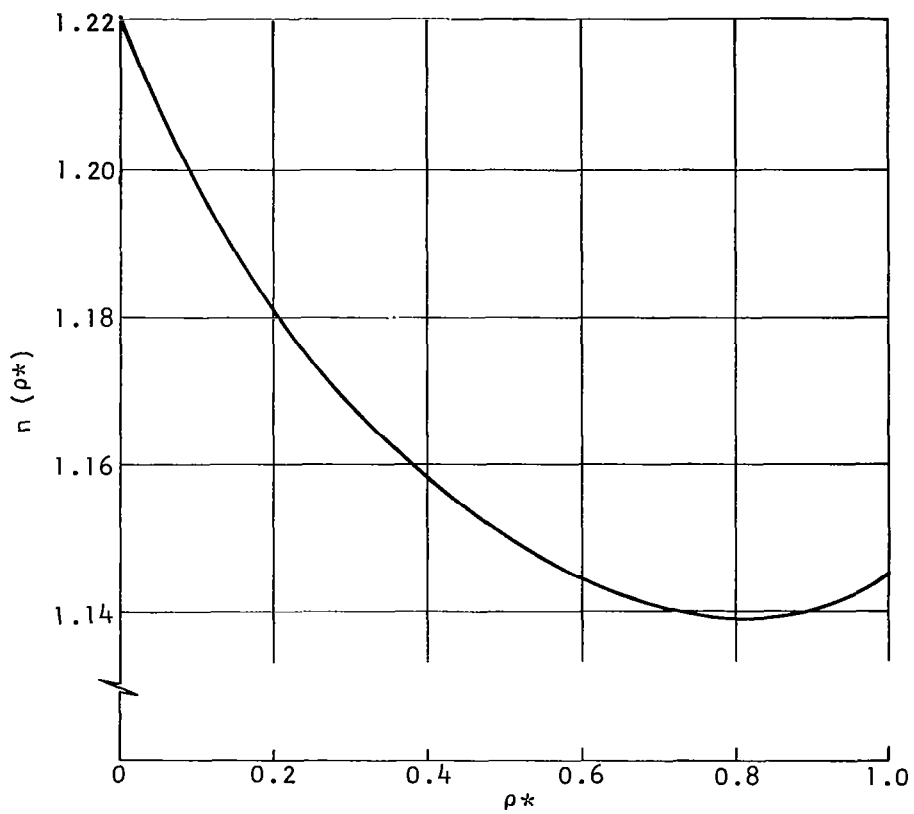
Fig. 8. Normalization Function n (ρ*)

SYMBOL	P	EXCITATION	f(Hz)
○	0	CROWN	48.9
⊖	0	HUB	48.7
□	6	CROWN	61.1
⊟	6	HUB	61.3
△	15	HUB	75.8
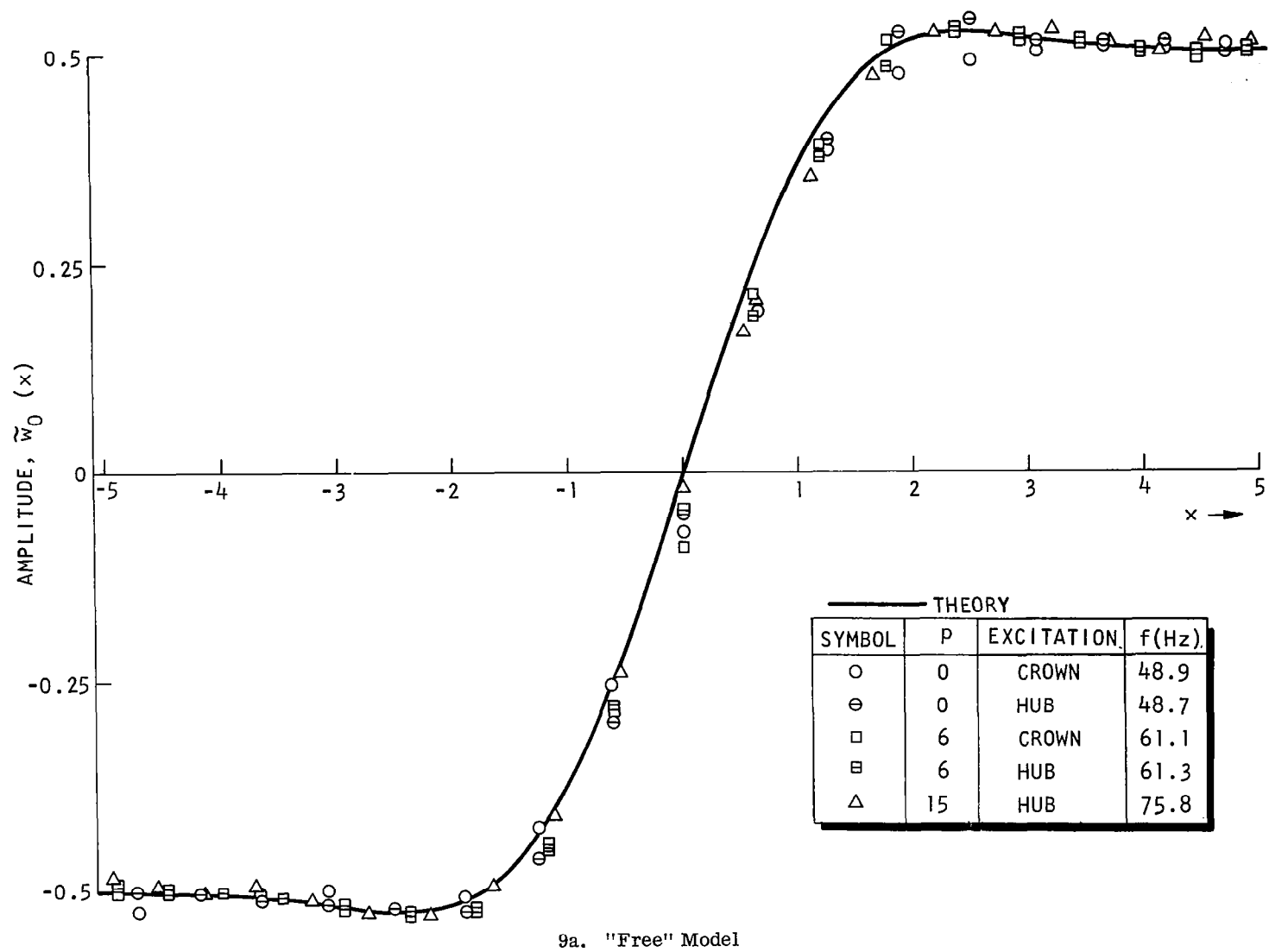
9a. "Free" Model

Fig. 9. Meridional Deformation in Fundamental Mode

AMPLITUDE, $\tilde{w}_0$ (x)

SYMBOL	P	HUB WEIGHT	f(Hz)
⊘	0	YES	24.1
□	6	NO	42.6
⊡	6	YES	30.1
△	15	NO	52.0
◁	15	YES	37.0

——— THEORY
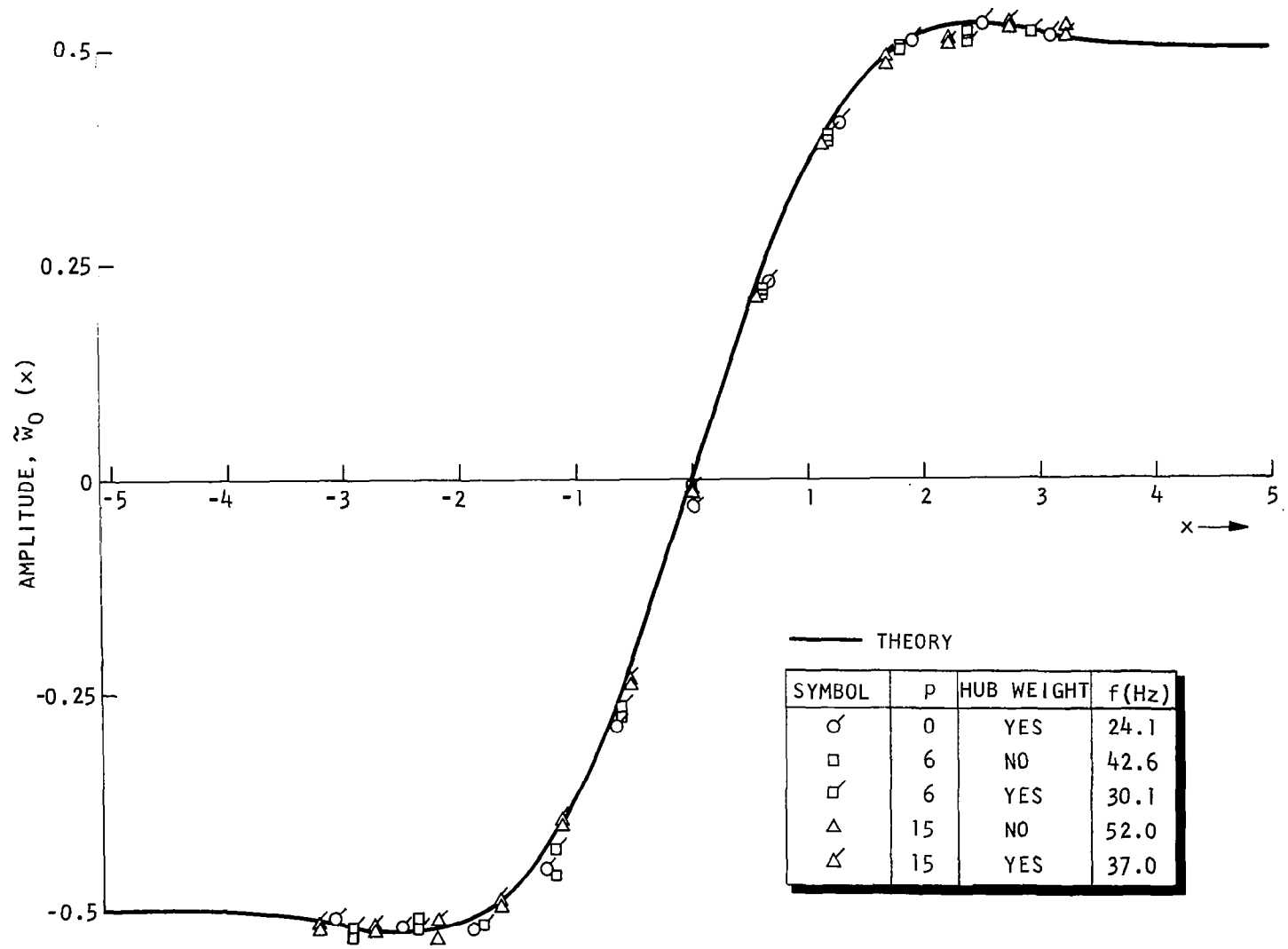
9b. "Fixed" Model

Fig. 9. (concluded)
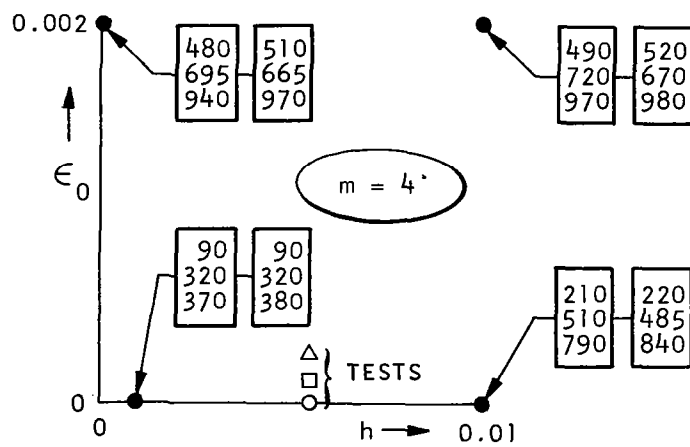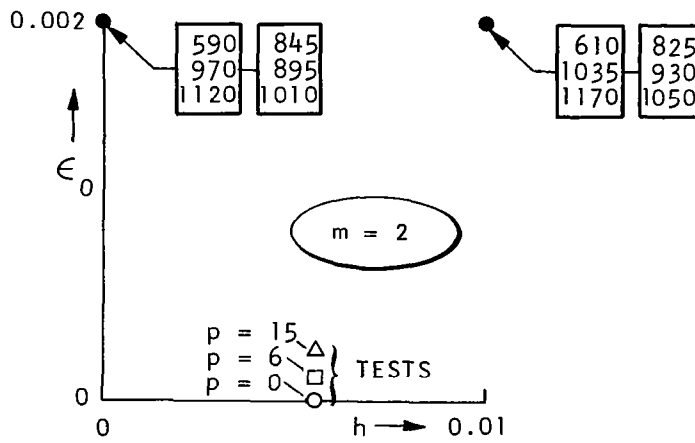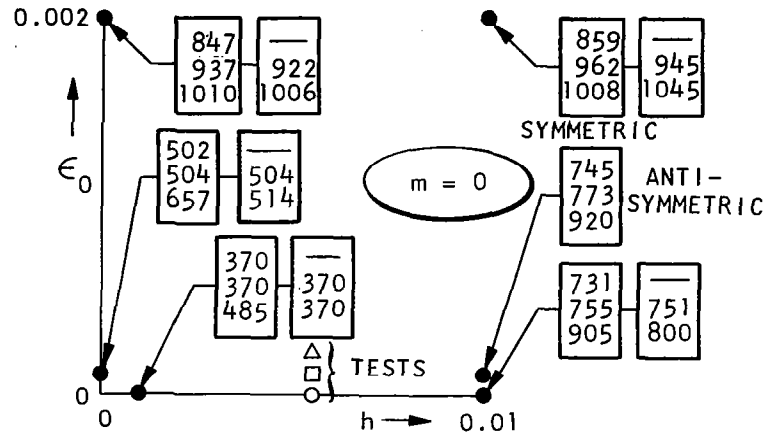
Fig. 10. Resonance Frequencies, Analytical Results (Ref. 3)
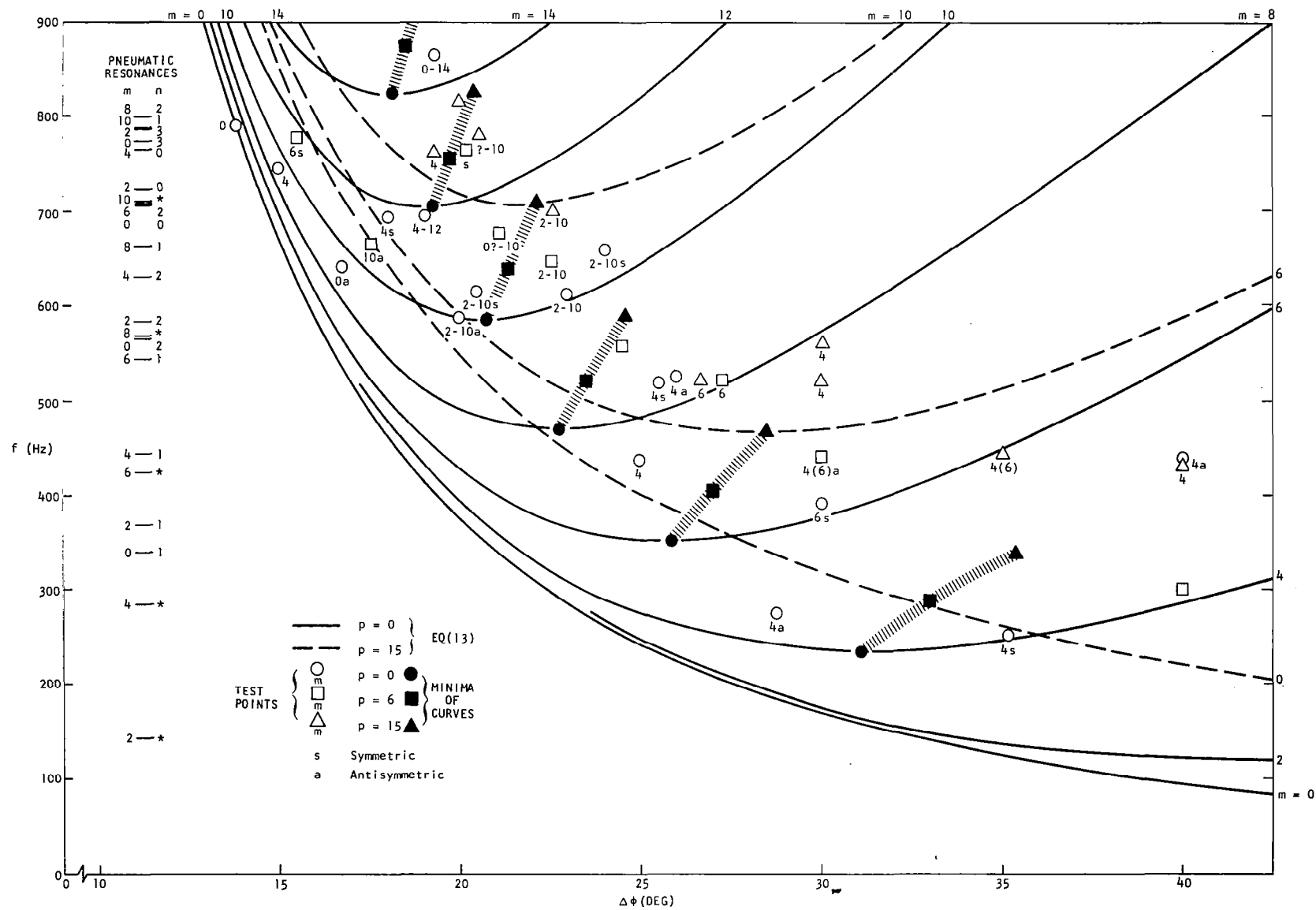
11a. "Free" Model

Fig. 11. Test Results, Frequency f over Distance Between Nodes $\Delta\phi$
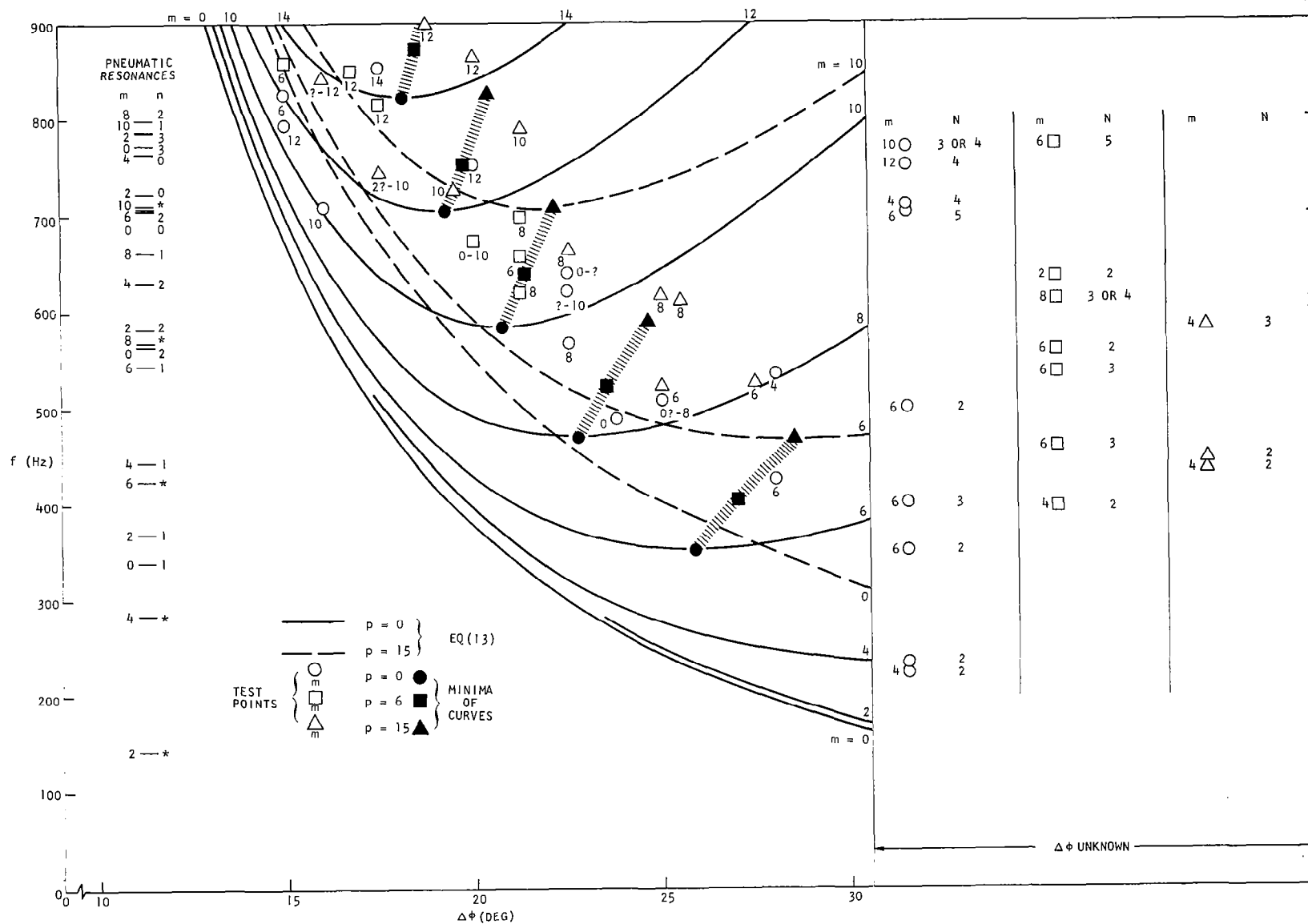
11b. "Fixed" Model

Fig. 11. (concluded)

a-1. Pressure Transducer, Air

a-2. Pressure Transducer, Helium Plus Air

a-3. Shell Displacement Opposite Shaker ($\theta = 225°$), Air

a-4. Shell Displacement Opposite Shaker ($\theta = 225°$), Helium Plus Air
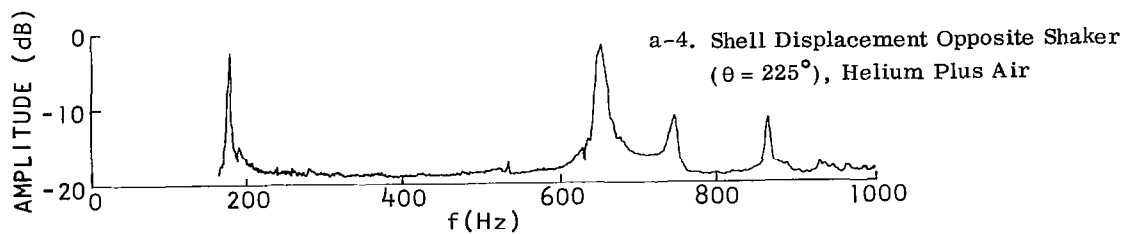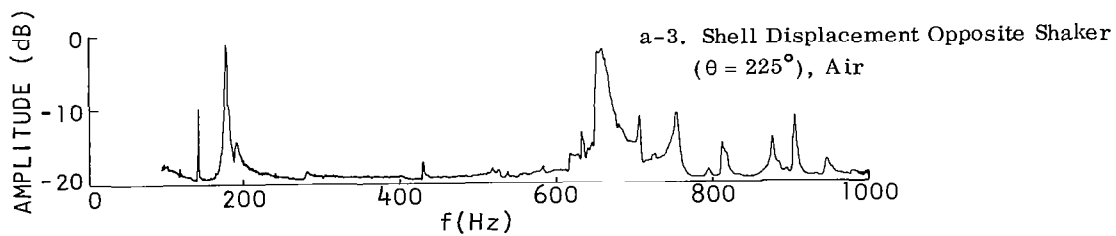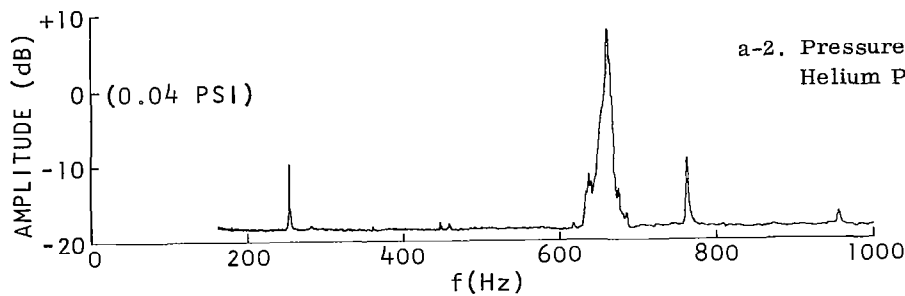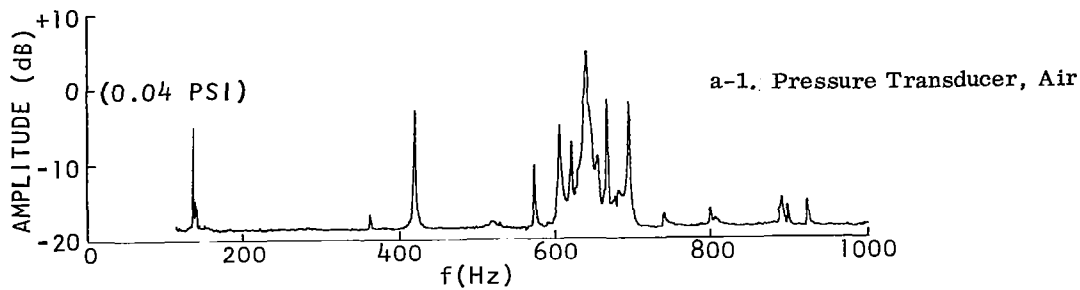
12a. Effect of Helium, Horizontal Excitation ($\phi = 90°$; $\theta = 45°$), p = 0,"Free"

Fig. 12. Spectrum Records

43

b-1. Pressure Transducer, Off-Crown Excitation

b-2. Displacement Off Crown, Off-Crown Excitation

b-3. Displacement Off Crown, At-Crown Excitation

b-4. Strain Gage Off Crown, At-Crown Excitation
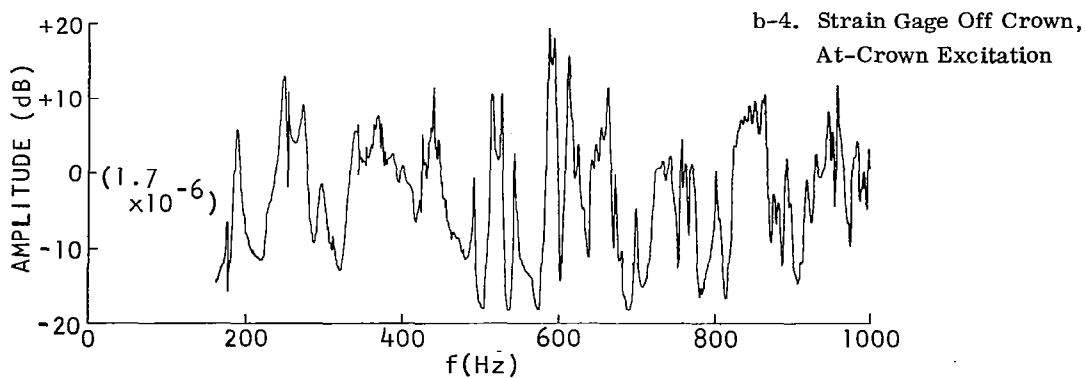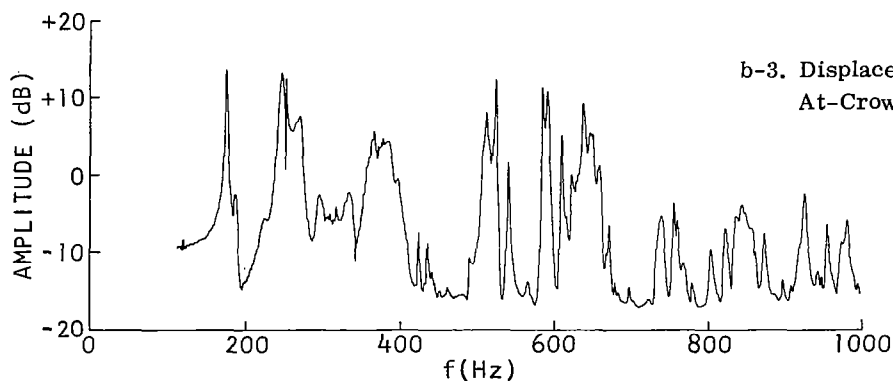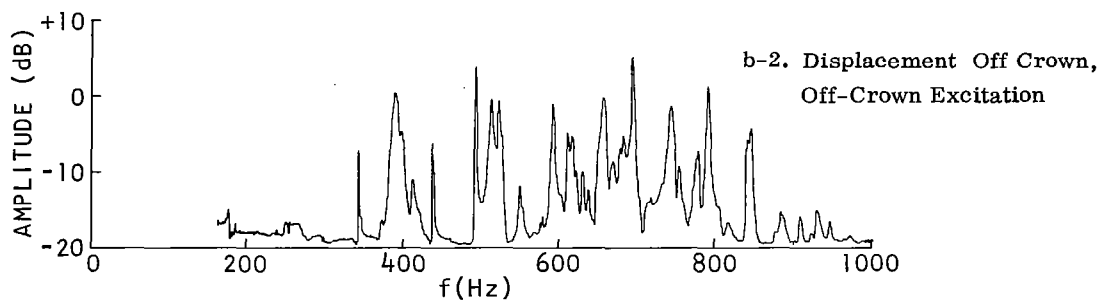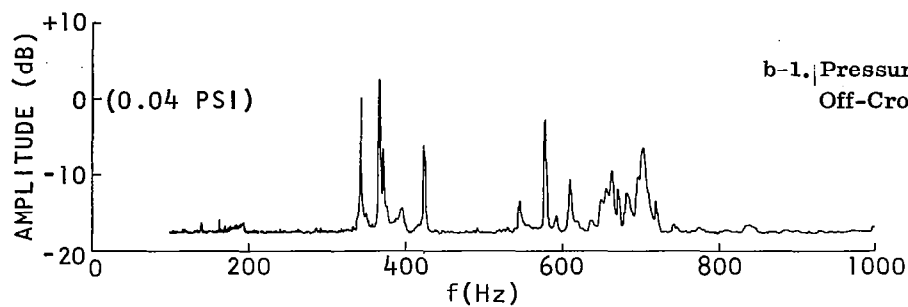
12b. "Free" Model, p=0, Excitation at Lower Half Shell

Fig. 12. (continued)

c-1. Pressure Transducer

c-2. Displacement Off Crown

c-3. Strain Gage at Crown
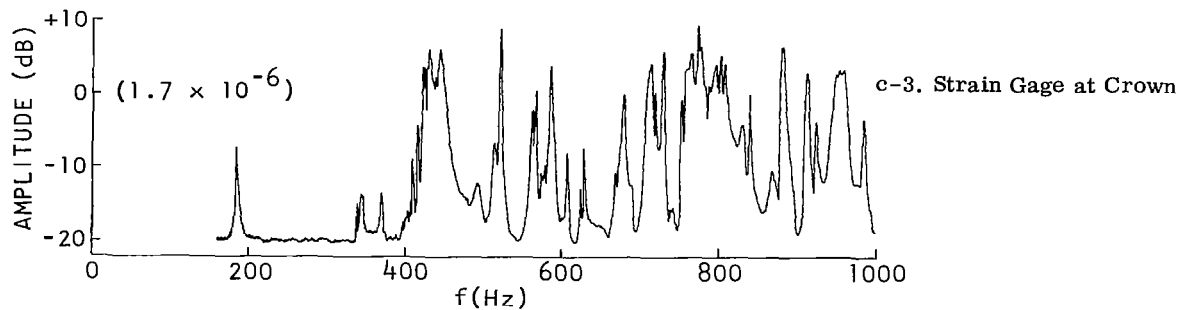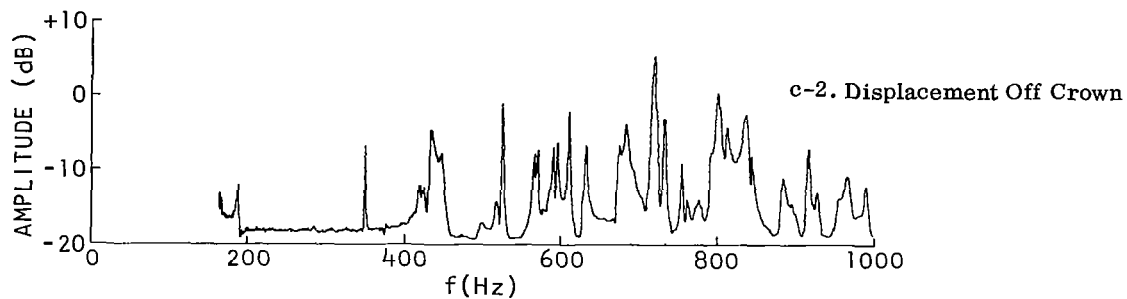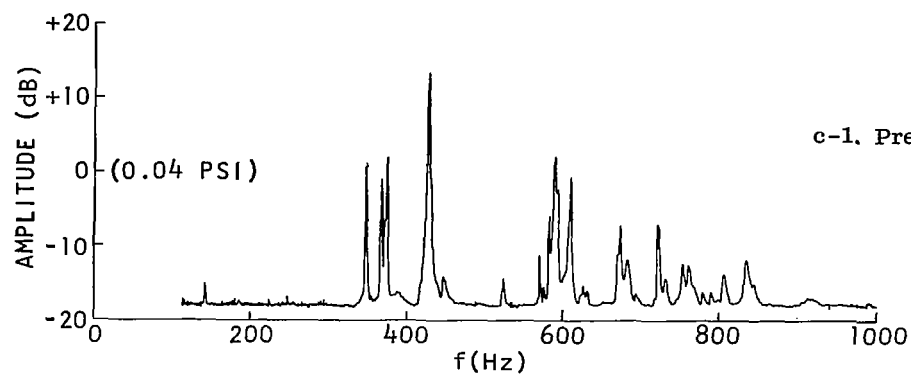
12c. "Free" Model, p = 15, Off-Crown Excitation at Lower Half Shell
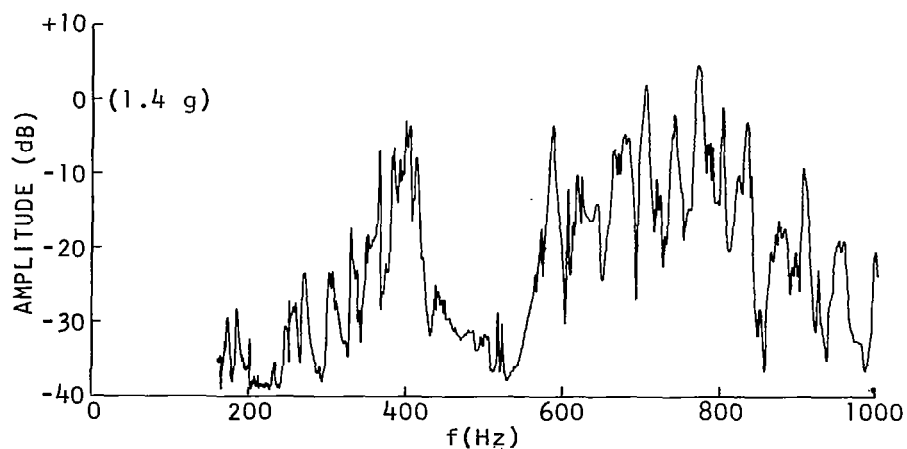
12d. "Fixed" Model, p = 15, Lateral Response of Support Lugs.
Excitation Off Upper Crown

Fig. 12. (concluded)

45
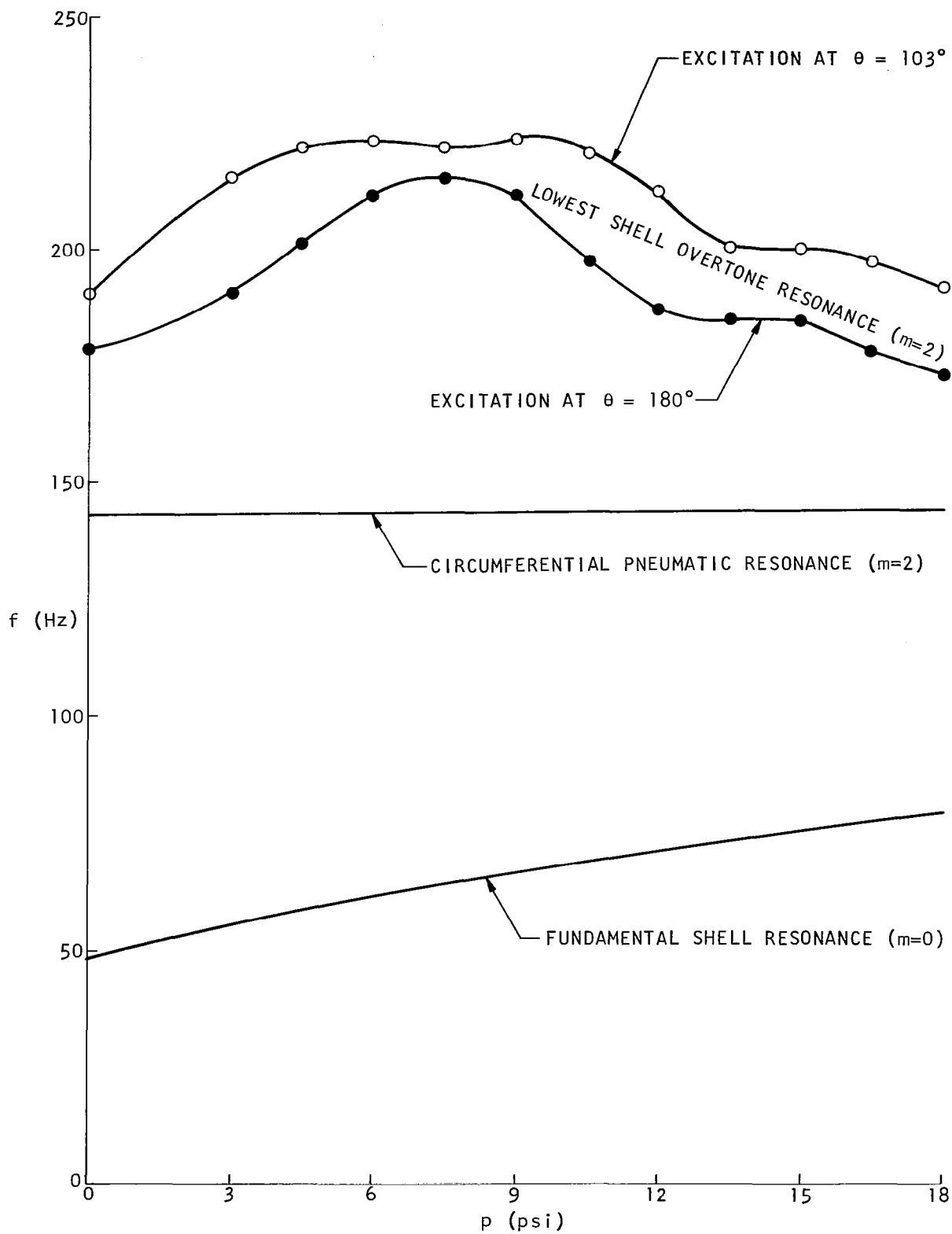
Fig. 13. Lowest Resonance Frequencies, "Free" Model
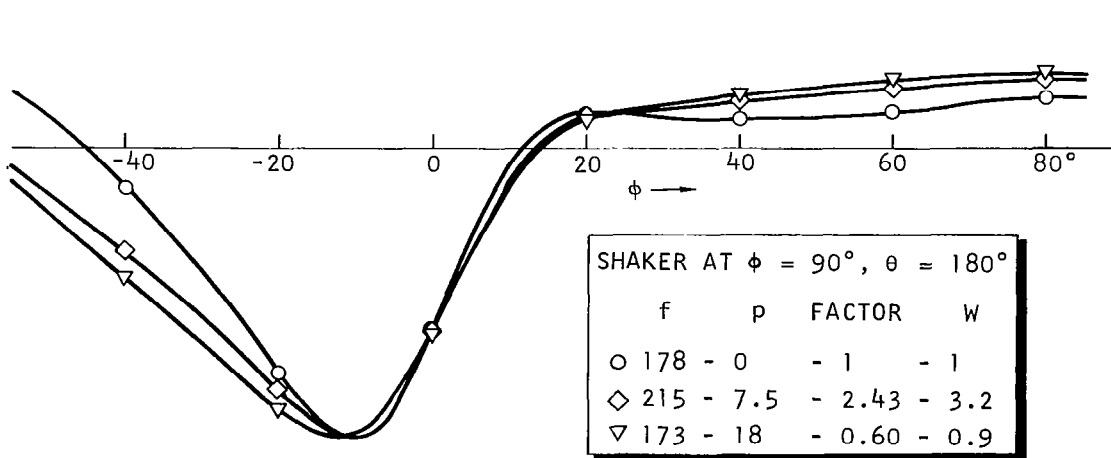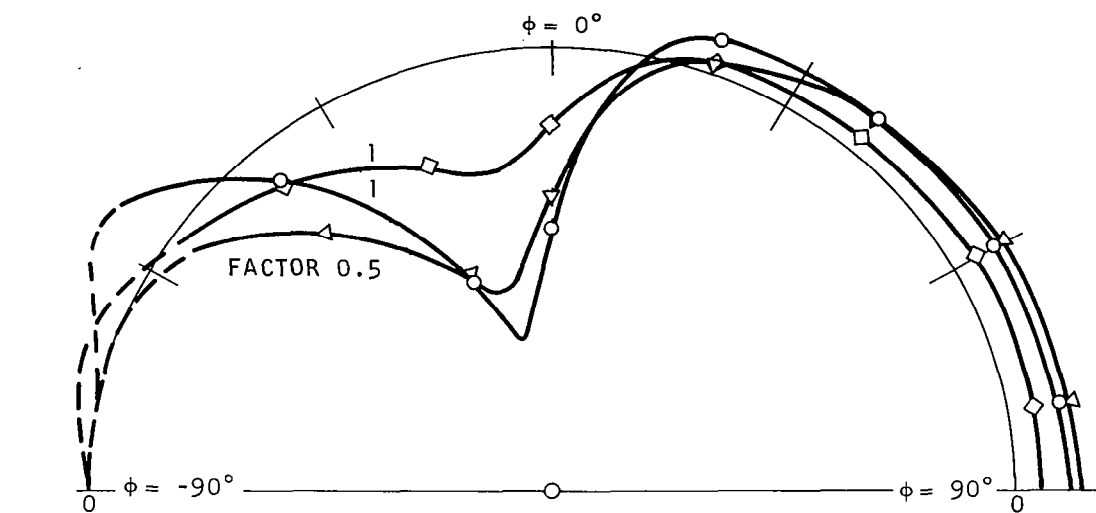
Fig. 14. First Overtone Mode (symmetric, m = 2, lower split mode). Measured Meridional Modal Shapes
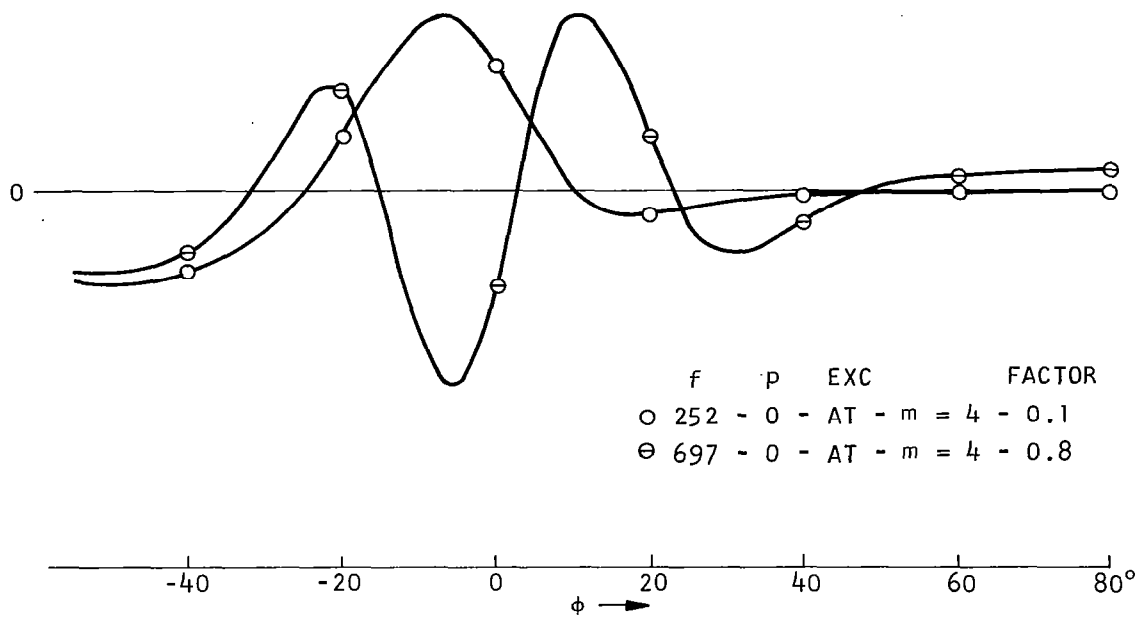
15a. m = 4 Modes
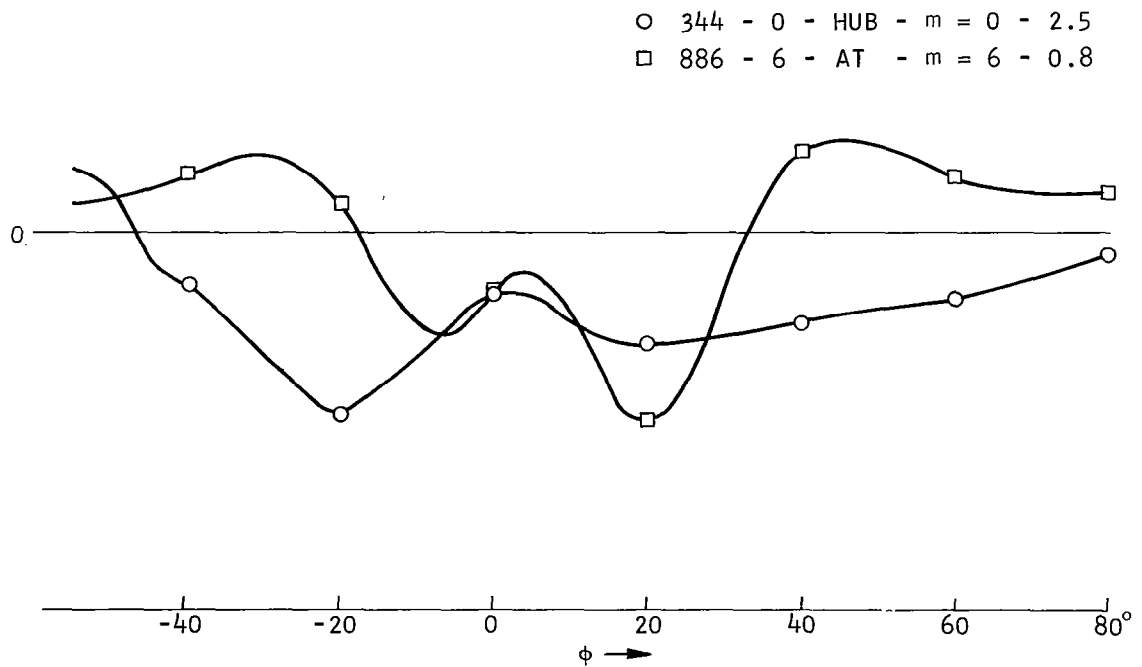
15b. Modes Showing Strong Pneumatic Effects

Fig. 15. Further Meridional Modal Shapes

Q 524 - 0 - OFF - m = 4 - 1
□ 523 - 6 - AT - m = 4 - 0.2
△ 519 - 15 - AT - m = 6 - 1

$\phi \longrightarrow$

15c. f ≈ 520 Modes

Q 592 - 0 - OFF - m = 2-10 - 0.4
○ 610 - 0 - AT - m = 2-10 - 0.4
□ 644 - 6 - AT - m = 2-10 - 0.4
△ 703 - 15 - AT - m = 2-10 - 1

$\phi \longrightarrow$

15d. m = 2-10 Modes
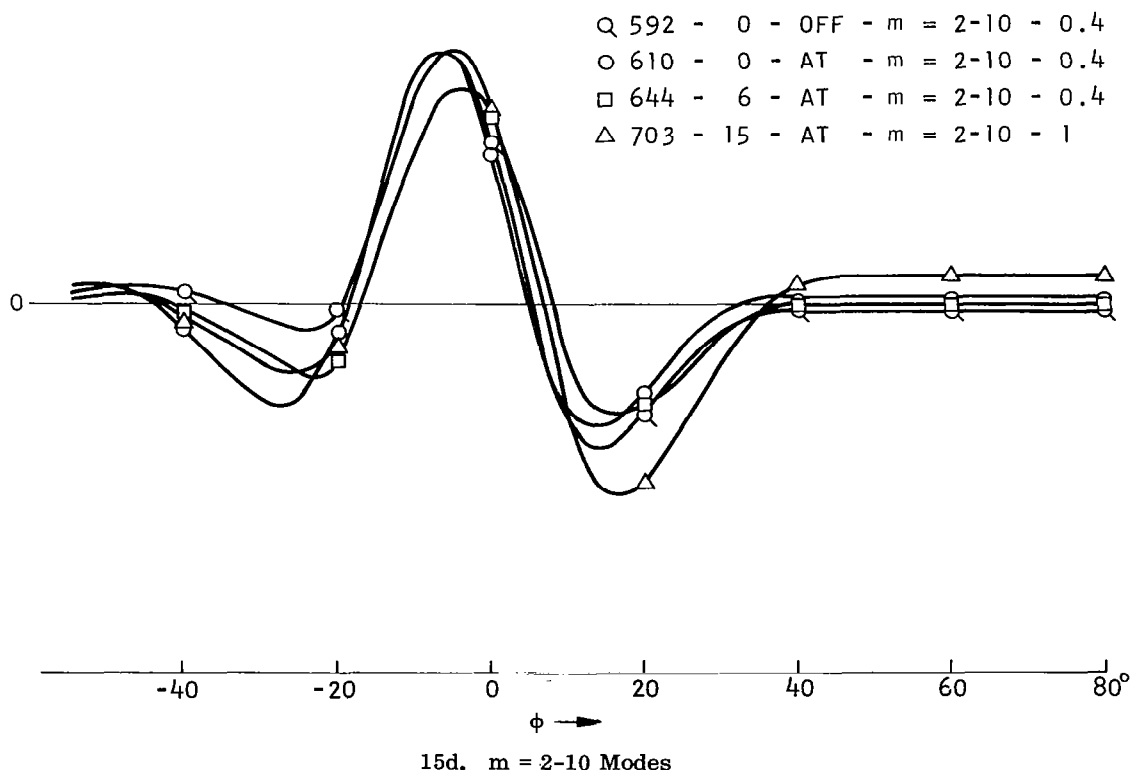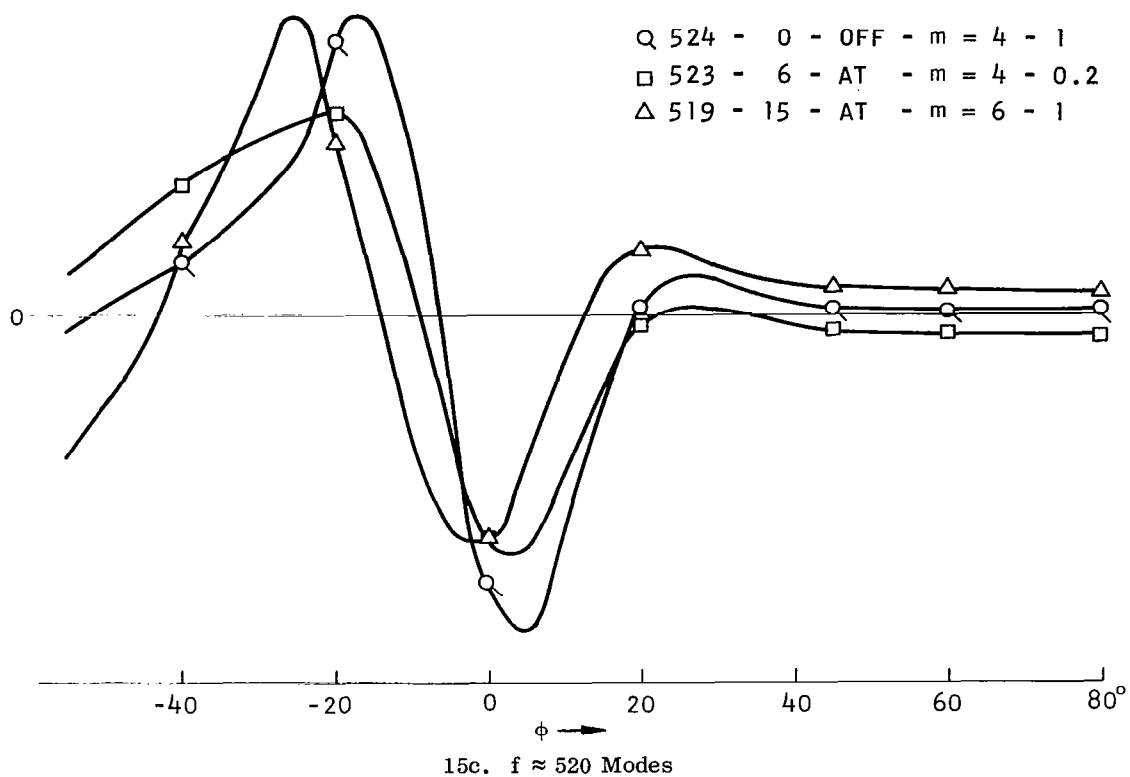
Fig. 15. (concluded)

$$\overset{*}{\underset{438}{f}} - \frac{p}{0} - \text{"FREE"} - \frac{EXC}{OFF} - m = 4$$

*NOTE:

THE IDENTIFICATION SEQUENCE
PLACED BESIDE EACH OF THE
FOLLOWING PHOTOGRAPHS COR-
RESPONDS TO THAT SHOWN BESIDE
THE FIRST PHOTOGRAPH ON THIS
PAGE AND, THEREFORE, THE
HEADINGS WERE NOT REPEATED ON
SUBSEQUENT PHOTOGRAPHS.
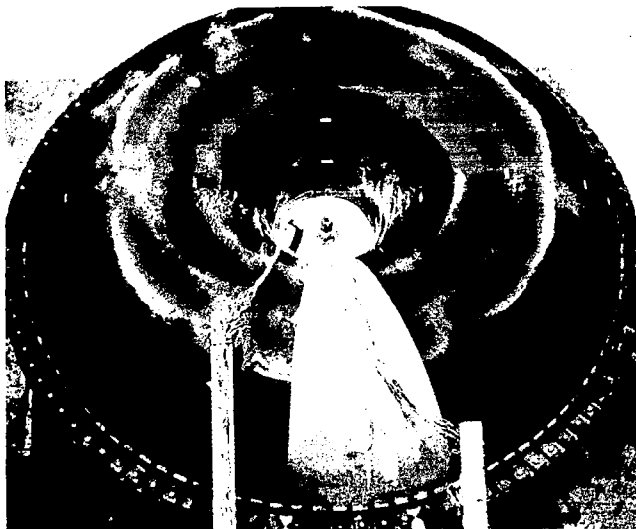
$$489 - 0 - \text{"FIXED"} - \text{OFF} - m = 0$$

Fig. 16. Photographic Records of Nodal Patterns, Ordered According
to Frequency f
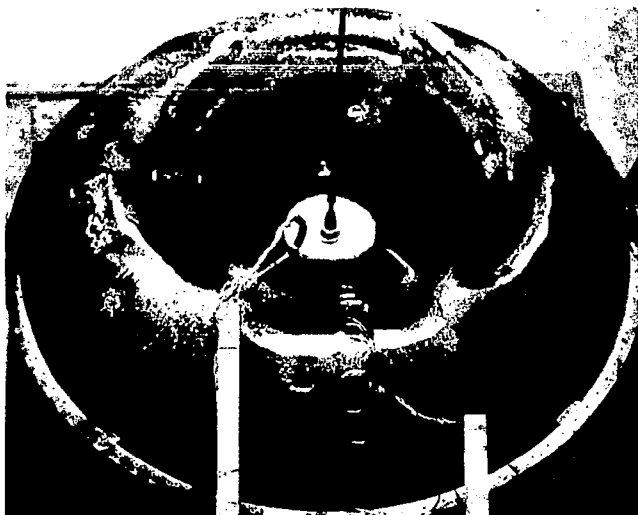
519 - 15 - "FREE" - AT - m = 6

523 - 6 - "FREE" - AT - m = 4
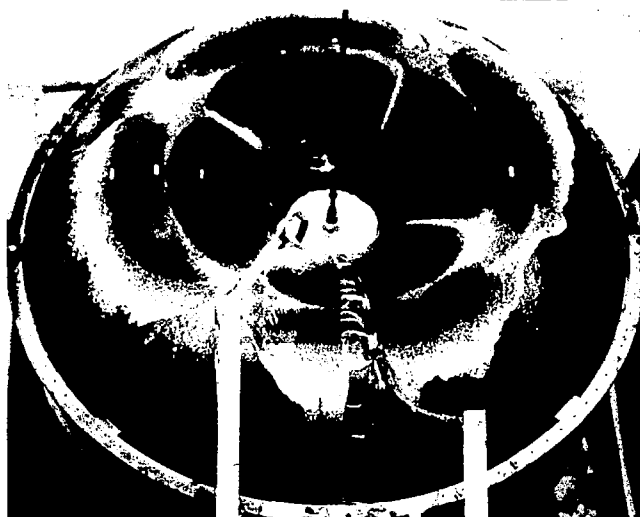
565 - 15 - "FREE" - AT - m = 4

Fig. 16. (continued)
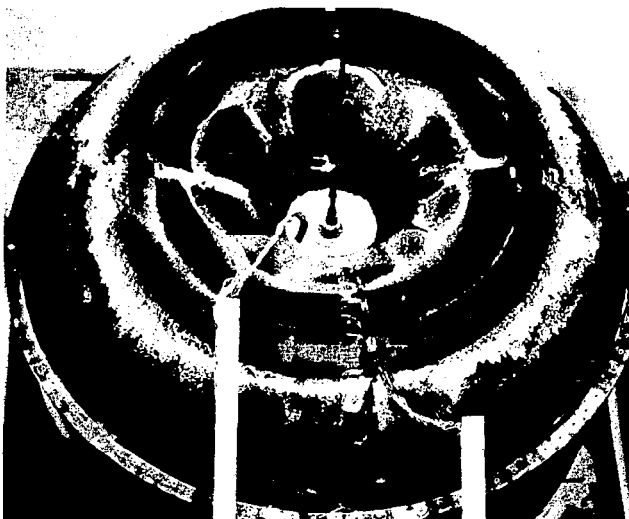
592 - 0 - "FREE" - OFF - m = 2-10

606 - 0 - "FREE" - AT - m = 2-10
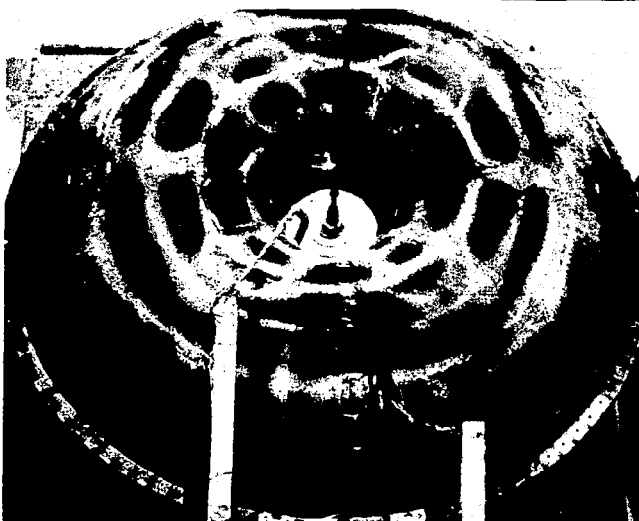
610 - 0 - "FREE" - AT - m = 2-10

Fig. 16.   (continued)
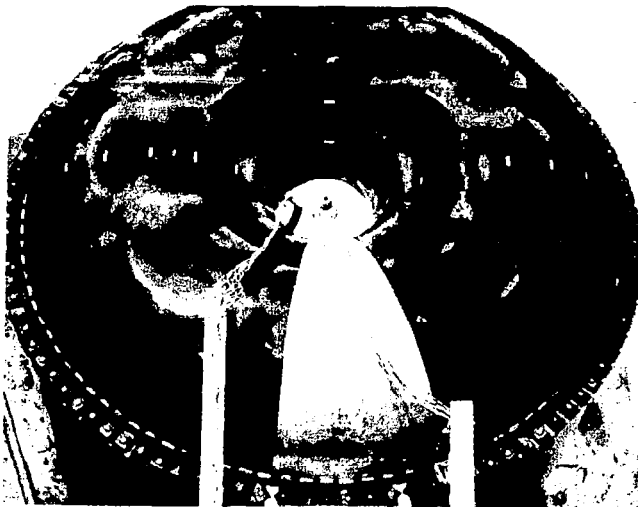
612 - 15 - "FIXED" - AT - m = 8
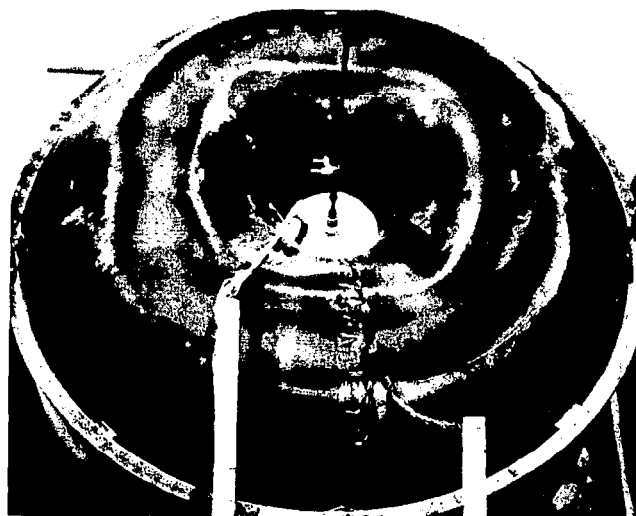
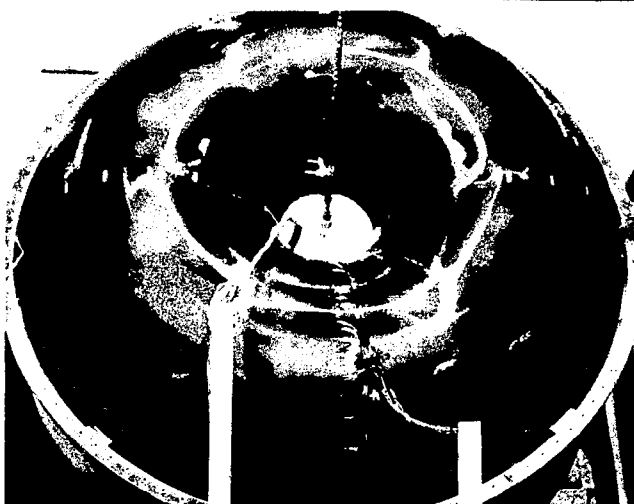644 - 6 - "FREE" - AT - m = 2-10
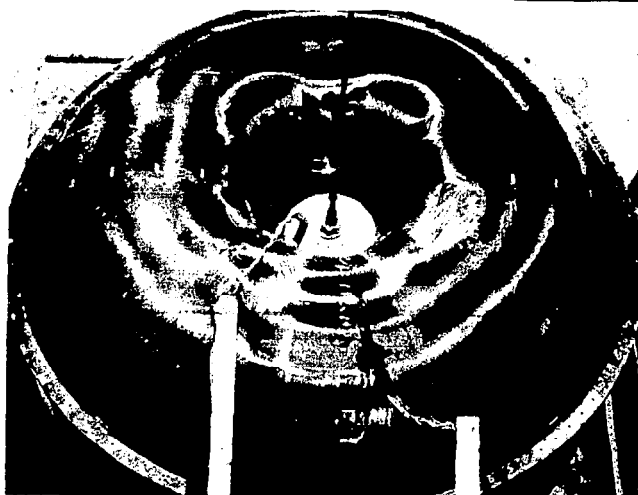
660 - 0 - "FREE" - AT - m = 2-10
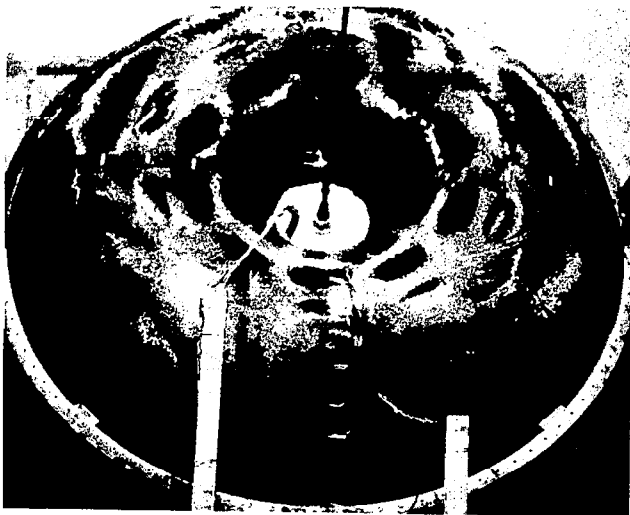
Fig. 16. (continued)

676 - 6 - "FREE" - AT - m = 0-10

705 - 0 - "FIXED" - AT - m = 10

775 - 6 - "FREE" - AT - m = 6
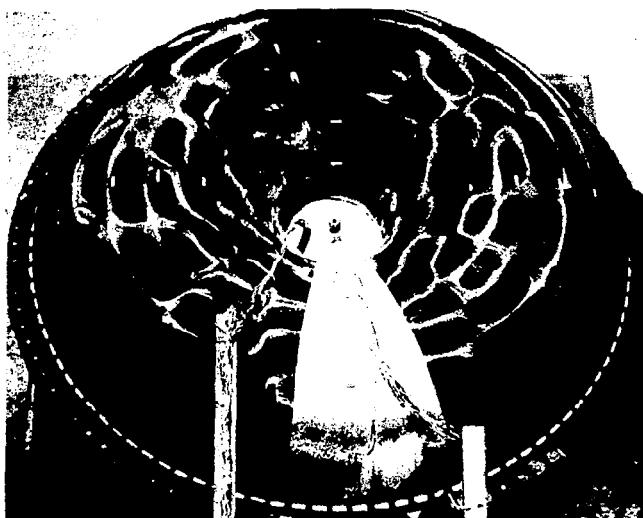
Fig. 16. (continued)

775 - 15 - "FREE" - AT - m = 10

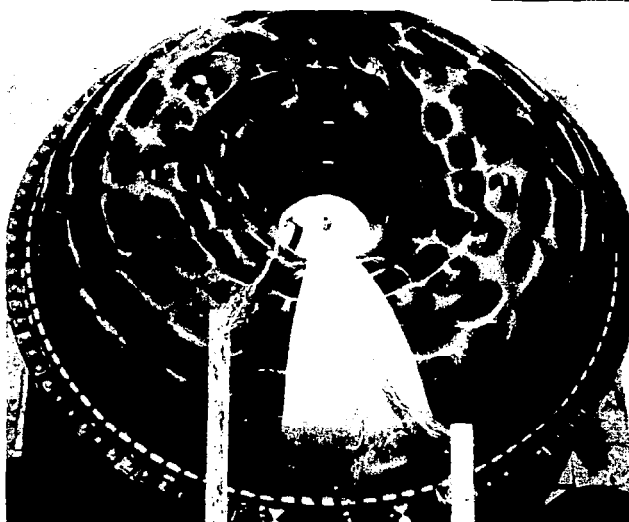856 - 0 - "FIXED" - OFF - m = 14

862 - 0 - "FREE" - AT - m = 14

Fig. 16. (continued)

55

990 - 0 - "FIXED" - OFF - m = 16

1105 - 15 - "FIXED" - OFF - m = 16
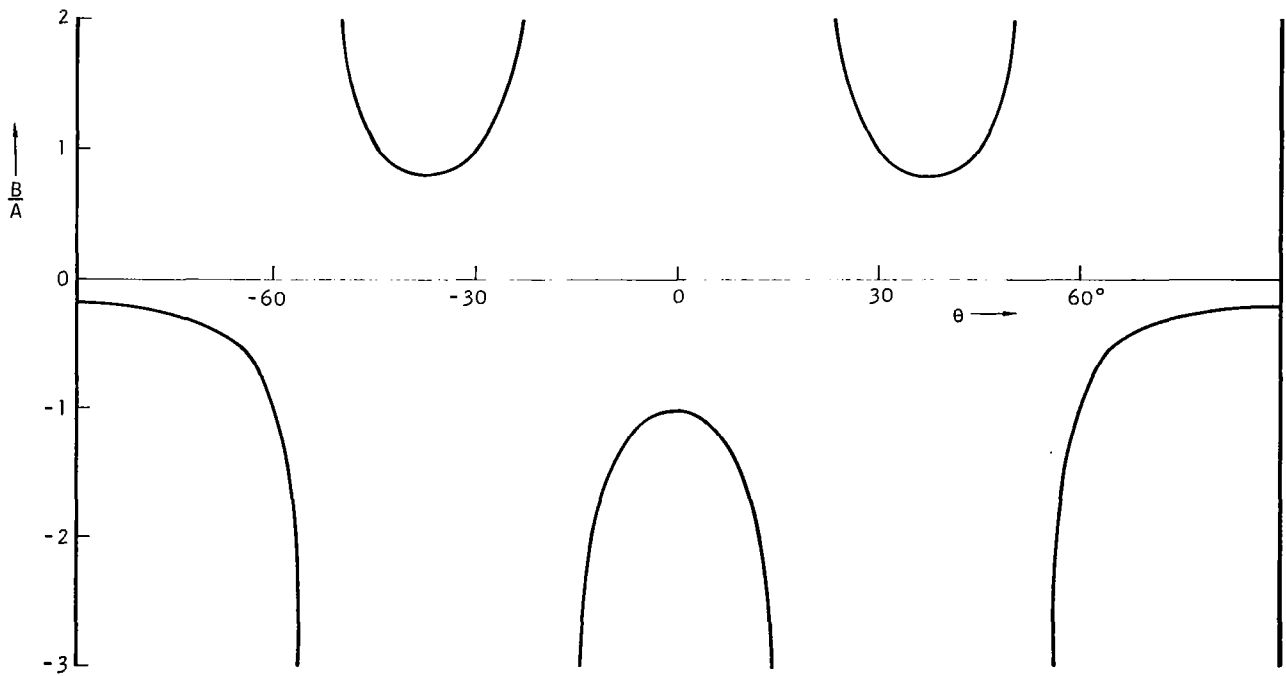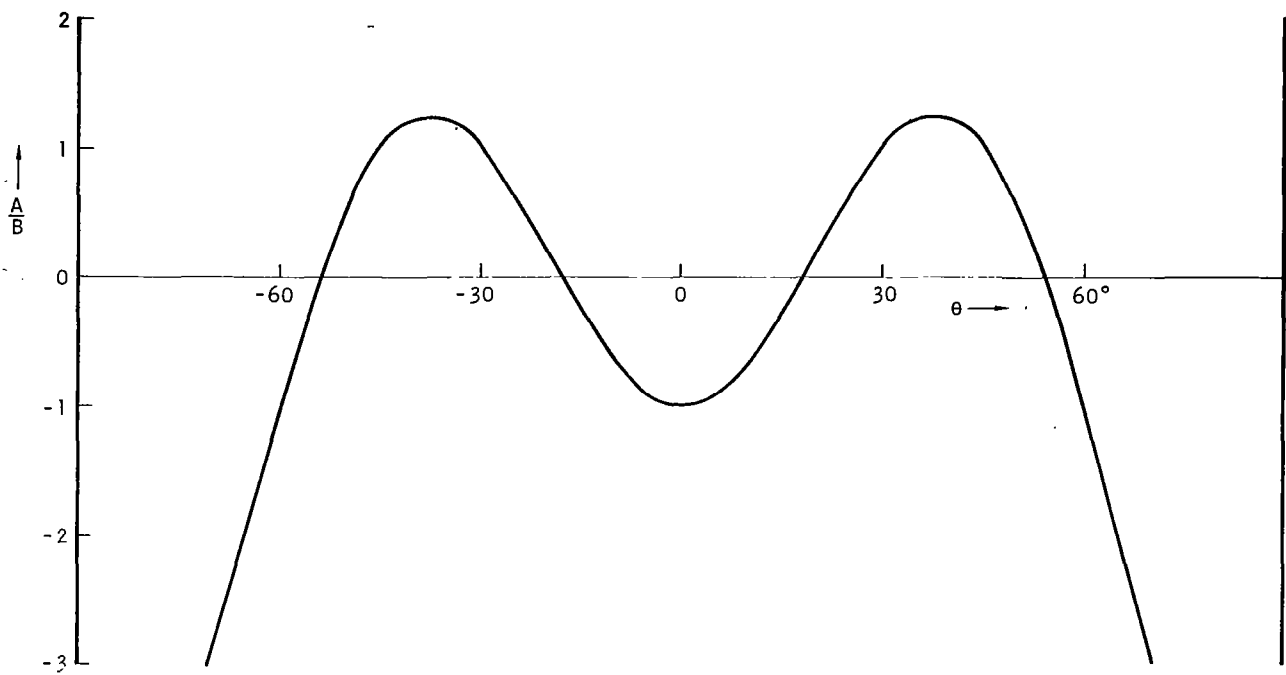
1211 - 15 - "FIXED" - OFF - m = 18

Fig. 16. (concluded)

56

Fig. 17. Roots of the Equation A cos θ + B cos 5θ = 0

"The aeronautical and space activities of the United States shall be conducted so as to contribute . . . to the expansion of human knowledge of phenomena in the atmosphere and space. The Administration shall provide for the widest practicable and appropriate dissemination of information concerning its activities and the results thereof."

—NATIONAL AERONAUTICS AND SPACE ACT OF 1958

NASA SCIENTIFIC AND TECHNICAL PUBLICATIONS

TECHNICAL REPORTS: Scientific and technical information considered important, complete, and a lasting contribution to existing knowledge.

TECHNICAL NOTES: Information less broad in scope but nevertheless of importance as a contribution to existing knowledge.

TECHNICAL MEMORANDUMS: Information receiving limited distribution because of preliminary data, security classification, or other reasons.

CONTRACTOR REPORTS: Scientific and technical information generated under a NASA contract or grant and considered an important contribution to existing knowledge.

TECHNICAL TRANSLATIONS: Information published in a foreign language considered to merit NASA distribution in English.

SPECIAL PUBLICATIONS: Information derived from or of value to NASA activities. Publications include conference proceedings, monographs, data compilations, handbooks, sourcebooks, and special bibliographies.

TECHNOLOGY UTILIZATION PUBLICATIONS: Information on technology used by NASA that may be of particular interest in commercial and other non-aerospace applications. Publications include Tech Briefs, Technology Utilization Reports and Notes, and Technology Surveys.

Details on the availability of these publications may be obtained from:

SCIENTIFIC AND TECHNICAL INFORMATION DIVISION

NATIONAL AERONAUTICS AND SPACE ADMINISTRATION

Washington, D.C. 20546